Montanuniversität Leoben

Influence of the bilayer period on the structure of AlN and the mechanical properties of CrN/AlN superlattice coatings

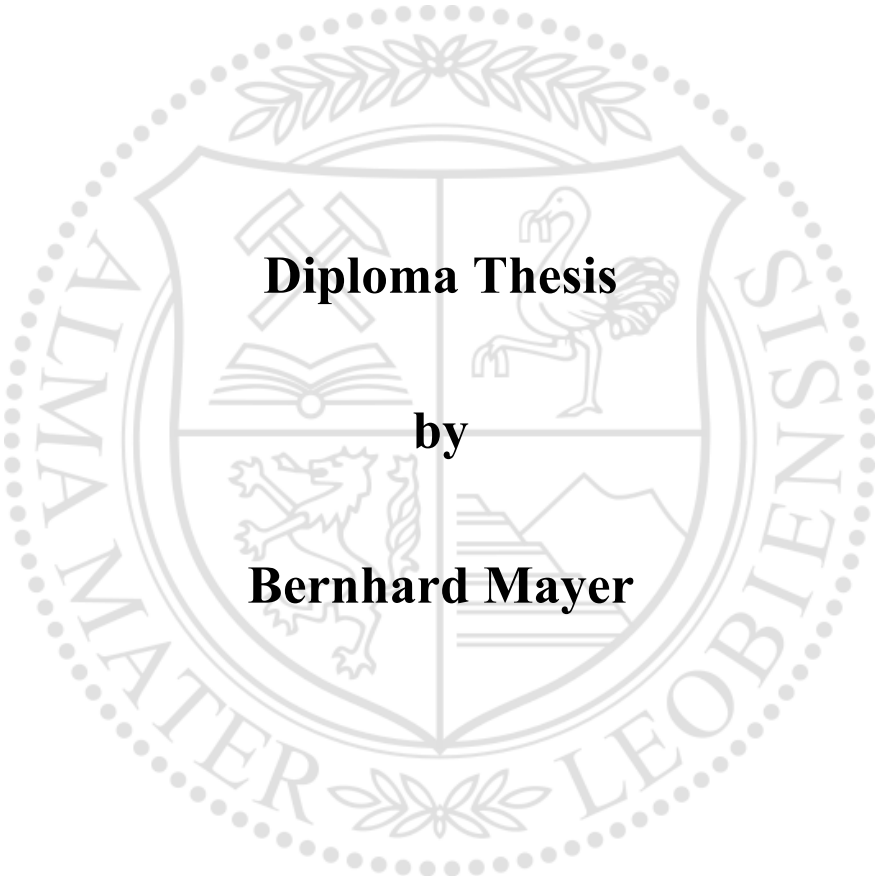

Diploma Thesis

by

Bernhard Mayer

Leoben, October 2012

This thesis was supported by the FWF START project (Y371) and the Förderstipendium of the Institute of Mathematics and Statistics at the University of Leoben.

Affidavit:

I declare in lieu of oath, that I wrote this thesis and performed the associated research by myself, using only literature cited in this volume.

Leoben, October 2012

Acknowledgements

First of all, I am very grateful to my Professor **Paul Mayrhofer** for his support and trust. About two years ago you offered me the possibility to start working on the basics of thin films as an assistant for PhD students. It so happened that a topic arose, which you offered me as a diploma thesis. Beside of this, you always found a minute to talk about problems or the latest result. And even in the conclusion phase of my thesis, where you schedule was really dense, you corrected my thesis in such a lovely manner. I wish you a good start at the Vienna University of Technology and congratulate you to your career structure.

In the same line I want to express my gratitude to the man who taught me and answered all my questions about theory and practice in the world of thin films, **Manfred Schlögl**. I was your first diploma student but you guided me through my thesis in the manner of a friend. I will never forget the times we spent together with "Angie" and the discussions about her being. Finally you corrected my written work several times with calm and precision. Especially, therefore thank you very much.

Furthermore I want to thank **Jörg Paulitsch** who answered tricky questions about my results and always supported me. Moreover, you helped me with my poster for the conference in Lausanne at the very last minute. I know you don't like it if someone comes to you at last minute, but you were very patient. Without your hints and modifications I would not like the poster so much.

I am also grateful to **my colleagues** and Co-diploma-students **Christian Koller** and **Helmut Riedl** within the **Thin Films Group** at the **Department of Physical Metallurgy and Materials Testing**. I will never forget the funny times at the coffee room or after work.

I was a member of a students' living community (boys & girls) at the Hauptplatz in Leoben, where I found friends for life. **Gernot Eggbauer**, **Christian Leodolter**, **Gerhard Peuker** and at this point I have to name him a second time as we do a lot of stuff together, **Helmut Riedl**. These guys were my family in Leoben and had always time for whatever. I really don't know how many parties we celebrated or how many beers we drunk, but I think it was more

than one. Thank you for the last five years and I am looking forward spending time together in the future.

At home in the wonderful village Grossengersdorf lives **my family**. I have to thank my mother, my father and even my brother for their support. Bringing me to or picking me up from the railway station are just examples of your numerous helping tasks.

A few months ago a girl entered my life and now I want to thank her at last but not least. It is to **Christina**, who backed me up and encouraged me to finish my study. Without any complaint you endured waiting for me, while I was working on my thesis. Special thanks to you and I am really looking forward to my future with you.

Table of Contents

Abstract **1**

Kurzfassung **2**

1 Introduction **4**

2 PVD – Physical Vapour Deposition **5**

2.1 Sputter Deposition 6

2.1.1 Glow discharge *6*

2.1.2 Reactive and non-reactive sputtering *9*

2.2 Film formation 9

2.2.1 Nucleation and film growth *9*

2.2.2 Structure zone models *11*

3 Coating system **13**

3.1 Chromium nitride – CrN 13

3.2 Aluminium nitride – AlN 15

3.3 Multilayer coatings 15

3.4 Superlattice coatings 16

4 Characterization Techniques **19**

4.1 X-ray diffraction 19

4.1.1 Low angle X-ray diffraction – LAXRD *19*

4.1.2 High angle X-ray diffraction – HAXRD *21*

4.2 Transmission electron microscopy (TEM) 23

4.3 Nanoindentation 24

4.4 Biaxial stress measurement 25

5 Deposition system **26**

6 Bibliography **27**

7 Publication **32**

Abstract

In the last years the research on CrN/AlN multilayer films has shown improved mechanical properties and oxidation resistance. Particularly CrN/AlN superlattice coatings show increasing hardness for a certain bilayer period (Λ). To obtain this superlattice structure both layer materials (CrN and AlN) have to exhibit the same crystal structure and a similar lattice parameter. The hardening effect corresponds to the metastable cubic (c) AlN phase, which is stabilized by coherency strains. However, a systematic study on the influence of the individual layer thicknesses of CrN and AlN on structural and mechanical properties of CrN/AlN superlattice coatings is still missing. Therefore, CrN/AlN multilayer coatings were prepared by DC reactive magnetron sputtering with AlN layer thicknesses of 1, 2, and 3.3 nm and varying the CrN layer thicknesses from 0.9 to 10 nm. The thereby obtained bilayer period and structure of the CrN/AlN coatings was investigated by low-angle and high-angle X-ray diffraction (LAXRD and HAXRD) as well as high-resolution transmission electron microscopy (HRTEM). The hardness as a function of Λ was determined with an ultra-micro-indentation system and the residual stresses were obtained by the substrate-curvature method at room temperature.

The results suggest that the minimum CrN layer thickness, necessary to stabilize the AlN layers in their metastable cubic structure, is in the range of the AlN layer thickness themselves. Hence, for the CrN/AlN coatings composed of 1, 2, and 3.3 nm thin AlN layers the CrN layers need to be at least 1, 2, and ~3 nm, respectively. For thinner CrN layers an X-ray amorphous structure or a multiphase arrangement of cubic, wurtzite-like, and amorphous phases is obtained. Exemplarily, the CrN/AlN superlattice coating composed of 1 nm thin AlN and 1.9 nm thin CrN layers (Λ = 2.9 nm) was investigated by cross-sectional HRTEM. These studies confirmed the superlattice structure–suggested by LAXRD and HAXRD–by the almost perfect hetero-epitaxial relationship between c-CrN and c-AlN. This CrN/AlN superlattice coating, as well as the one composed of 2 nm thin AlN and 3.5 nm thin CrN (Λ = 5.5 nm) exhibit a hardness maximum of ~31 GPa. If the AlN layer thickness is ~3.3 nm the hardness peak is obtained only with ~28.5 GPa for a bilayer period of Λ = 6.3 nm. The resulting hardness-peak as a function of the bilayer period becomes broader with increasing AlN layer thickness. A corresponding dependence on the bilayer period is also obtained for the compressive stresses.

Based on the results it can be concluded that the arrangement of 1 nm thin AlN layers with 1.9 nm thin CrN layers or 2 nm thin AlN layers with 3.5 nm thin CrN layers will result in the formation of a superlattice CrN/AlN structure having a hardness of ~40 % above that of the layers they are formed.

Kurzfassung

In den letzten Jahren zeigte die Forschung im Bereich von CrN/AlN Mehrlagenschichten Verbesserungen bezüglich ihrer mechanischen Eigenschaften und ihrer Oxidationsbeständigkeit. Im speziellen weisen CrN/AlN Mehrlagenschichten mit einer Übergitterstruktur einen Anstieg ihrer Härte bei einem bestimmten Wert der Doppellagenperiode (Λ) auf. Diese Übergitterstruktur wird erreicht, wenn beide Lagenmaterialien (CrN und AlN) die gleiche Kristallstruktur und einen ähnlichen Gitterparameter zeigen. Der Härteeffekt geht mit der Bildung der metastabilen kubischen (c) AlN Phase einher, die durch Kohärenzspannungen ermöglicht wird. Eine systematische Studie, welche den Einfluss der individuellen Lagendicken von CrN und AlN auf die Struktur und mechanischen Eigenschaften von CrN/AlN Mehrlagenschichten mit Übergitterstruktur untersucht, fehlte allerdings. Aus diesem Grund wurden CrN/AlN Mehrlagenschichten mit AlN Lagendicken von 1, 2 und 3.3 nm und CrN Lagendicken zwischen 0.9 und 10 nm mittels reaktivem DC Magnetron Sputtern hergestellt. Die dabei erhaltene Doppellagenperiode und die Struktur der CrN/AlN Mehrlagenschichten wurden mittels Kleinwinkel und Großwinkel Röntgenbeugung (LAXRD und HAXRD) und hochauflösender Transmissions-elektronmikroskopie (HRTEM) untersucht. Ein Ultra-Micro-Indentations System wurde verwendet um die Härte zu messen. Diese wurde anschließend als Funktion der Doppellagenperiode aufgetragen, ebenso wie die Schichteigenspannungen die über eine Substratdurchbiegungsmethode ermittelt wurden.

Aus den Ergebnissen war zu folgern, dass eine minimale CrN Lagendicke notwendig ist, um die AlN Lagen in ihrer kubischen Struktur zu stabilisieren. Diese minimale CrN Lagendicke liegt im Bereich der AlN Lagendicke. Folglich wird für die CrN/AlN Mehrlagenschichten mit 1, 2 und 3.3 nm dünnen AlN Lagen eine CrN Lagendicken von 1, 2 und ~3 nm benötigt. Durch dünnere CrN Lagen kommt es zur Ausbildung einer röntgenamorphen Struktur oder

einer Mischung aus kubischen, wurtzit-ähnlichen und amorphen Phasen. Exemplarisch für alle CrN/AlN Mehrlagenschichten mit Übergitterstruktur wurde die Mehrlagenschicht mit 1 nm dünnen AlN und 1.9 nm dünnen CrN Lagen (Λ = 2.9 nm) mittels HRTEM untersucht. Diese Untersuchung bestätigte die Übergitterstruktur, wie sie bereits durch LAXRD und HAXRD angedeutet wurde, durch die Ausbildung einer nahezu perfekten hetero-epitaktischen Beziehung zwischen den c-CrN und c-AlN Lagen. Für diese CrN/AlN Mehrlageschicht mit Übergitterstruktur, ebenso wie für die Mehrlagenschicht bestehend aus 2 nm dünnen AlN und 3.5 nm dünnen CrN Lagen (Λ = 5.5 nm), wurde das Härtemaximum von ~31 GPa erreicht. Die Mehrlagenschichten bestehend aus 3.3 nm dünnen AlN Lagen weisen hingegen nur einen maximalen Härtewert von ~28.5 GPa auf, der bei einer Doppellagenperiode von Λ = 6.3 nm erreicht wird. Die Ausbildung des Härtemaximums in Abhängigkeit der Doppellagenperiode wird mit steigender AlN Lagendicke breiter. Diese Abhängigkeit wird auch bei den Eigenspannungswerten beobachtet.

Basierend auf unseren Ergebnissen kann abschließend gefolgert werden, dass die Mehrlagenschicht mit 1 nm dünnen AlN und 1.9 nm dünnen CrN Lagen oder jene mit 2 nm dünnen AlN und 3.5 nm dünnen CrN Lagen eine CrN/AlN Übergitterstruktur ausbilden und eine um ~40% höhere Härte als die entsprechenden Lagenmaterialien aufweisen.

1 Introduction

Materials science has always been the key for the wealth of human life and being. Especially upcoming materials like iron or bronze influenced and named times of history. The industrial revolution forced industry to invent and improve technologies and techniques for further progress. Therefore material science becomes more important to develop materials with increased e.g., mechanical and chemical properties in order to fulfil the requirements of the industry. This need in extended research activities resulted in new inventions and new materials, which enable high-tech products i.e. displays with a scratchproof touchscreen and cars with little fuel consumption and high efficiency [1,2]. And a key word for these investigations is nano-structures. During the last decades a lot of research concentred on the development of materials having a 0, 1, 2, or 3 dimensional nanostructure. Surfaces having nano-textures e.g., holes or dots are one-dimensional nanostructures. Further are nanotubes two-dimensional and e.g., spherical nanoparticles three-dimensional nanostructures. The focus of this thesis is concentrated on materials having a one-dimensional nanostructure. Especially with deposition techniques, such layered materials, for example, can conveniently be prepared by simply changing (or alternating) the evaporation sources (or sputter sources) during preparation when using a multiple source equipment. This will lead to multilayer coatings, composed of individual layers. If the individual layer thickness is in the range of a few lattice parameters, and the individual layers crystallize in the same structure with only a small difference in lattice parameter, superlattice coatings can be formed. When such coatings are composed by two different nm-thin layers, which alter in periodic manner, they are often characterized by the bilayer period Λ.

Depositing a coating on a tool is one useful technique to improve the properties of its surface in order to resist the environmental conditions during the working processes. Especially cutting inserts or drilling tools to machine different materials show improvements regarding output and lifetime, due to protecting the surface against wear and fatigue even at elevated temperatures. Hard coatings like CrN, TiN, $Ti_{1-x}Al_xN$ are well known and used as protective films, as they exhibit high thermal resistance combined with high wear resistance [3–7]. However, in recent years the thermal stability, oxidation resistance and mechanical properties of such coatings were the subject of many research activities due to the need of further improved coatings. For example by alloying such coatings like $Ti_{1-x}Al_xN$ with Y, Ta or Nb leads to increased thermal stability and mechanical properties [8,9].

In addition to alloy a coating material to synthesise ternary or multinary films for improved properties, also the architecture can be changed which can further modify the materials response against mechanical and thermal attack. Coatings composed of various layers, so-called multilayers were found to enhance the thermal and mechanical properties as well as increase the fracture toughness [10–12]. Within these multilayer coatings, parameters like the number of layers or interfaces, often characterized by the bilayer period Λ (the sum of the layer thicknesses of two alternating layers), and the crystal structure are influencing the properties of the coating [13–16].

2 PVD – Physical Vapour Deposition

In industry, physical vapour deposition (PVD) and chemical vapour deposition (CVD) are well-established techniques to deposit high quality thin films.

Unique benefits of CVD are the high deposition rate, uniform deposition and film thickness, even on substrates with complex geometry [17]. Basically, the film nucleation and growth is initiated at a heated surface by a chemical reaction of a gas mixture. The variation of the process parameters like temperature and gas mixture results in a wide range of modified CVD techniques. The relatively high temperature during the process leads to high-energy costs and limits the number of substrates to thermally stable ones, like cemented carbide [18].

PVD is a process, where a target material, either liquid or solid, is vaporized, by the use of plasma or high power current discharge, and then transported through a vacuum environment to condense at the substrate surface. Based on the technique used to vaporise the material, different PVD processes can be distinguished [19]:

- Thermal evaporation
- Sputtering
- Arc evaporation
- Laser ablation

With these methods it is possible to deposit metals, alloys or compounds either by non-reactive or reactive processes, using e.g., N_2 to form nitrides. In general, the temperature required for the PVD processes is with ~200 – 500 °C much lower than for the CVD process.

This allows film deposition on substrates with lower thermal stability and therefore opens a wide range of applications [18,19].

As sputter deposition is the choice of method for this thesis, this will be described in more detail in the following chapter.

2.1 Sputter Deposition

2.1.1 Glow discharge

The glow discharge enables the generation of ions due to an applied electric field. The thereby generated plasma acts as source for electrical charged particles, having random movement, and behaves like an ionized gas without charge, as negative and positive charged particles are in equilibrium. The required free charge carriers originate from the ionization of particles due to inelastic collisions. The inelastic collision of a free electron with a neutral particle results in a new ejected electron and ion. Next to this ionization various other processes can happen, like recombination of positive and negative charged particles or collisions with the chamber wall. The behaviour of charged particles during the discharge is described schematically by the current-voltage (I-V) characteristics in Figure 2.1 [18].

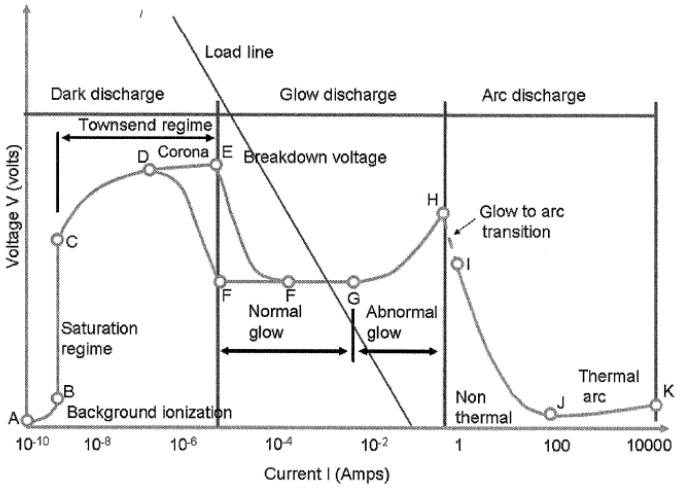

Figure 2.1: I-V characteristic of the discharge in a vacuum chamber [18].

Basically, the I-V characteristic is separated in three regions, the dark discharge, the glow discharge and the arc discharge resulting in different phenomena. The first region characterizes the dark discharge (A-E), which is invisible for the human eye. From point A to

B ions and electrons move toward the electrodes due to the applied electric field, generating a weak current. The current saturates from B to C due to a higher applied voltage resulting in a better collection efficiency of electrons and ions as all produced ions and electrons reach the electrodes. If the voltage is furthermore increased, the current raises strongly from C to E, which is characterized by the "Townsend regime". "Corona discharges" (D-E) can be identified as glow discharges in the "Townsend regime" before electrical breakdown. The electrical breakdown potential at point E results from a high electric field resulting in additionally emitted secondary electrons from the cathode. At this voltage the current may increase significantly, but is limited by the internal resistance of the power supply. Furthermore the breakdown voltage depends on the gas, the electrode material, the pressure and the distance between the electrodes. The following glow discharge from F to G has luminous character and is important for sputter deposition, separated in the normal (F-G) and the abnormal (G-H) glow discharge. The latter is the more important one for sputter deposition as the plasma is evenly distributed at the cathode and an increase of the voltage leads to an increase of the current. At point H the transition from glow discharge to arc discharge is indicated. Due to a rapid increase of current the cathode is heated and electrons are emitted thermally [18].

Argon (Ar) is mainly used as inert gas in the vacuum chamber and acts as source for ions (Ar^+). The most important process is an inelastic collision of an Ar atom with a free electron. This electron hits an electron of the outer shell of the Ar atom. Thereby an Ar^+ ion and an emitted electron e^- are generated, which are furthermore part of the ionization process (see Figure 2.2 (a)). Moreover, an accelerated ion with insufficient energy to sputter an atom from the target can hit an electron from an atom close to the target surface (see Figure 2.2 (b)). Figure 2.2 (c) illustrates the emission of secondary electrons from the anode due to the acceleration of an electron towards to the substrate. The interaction shown in Figure 2.2 (d) indicates the sputtering process, where an accelerated ion with sufficient energy hits the target and vaporizes an atom from the surface. The process shown in Figure 2.2 (e) represents the symmetric charge exchange, where an Ar^+ passes close (a few Å) an Ar atom. This nearly contact enables quantum mechanical tunnelling and allows the transfer of electrons resulting again in an atom and an ion [18,20].

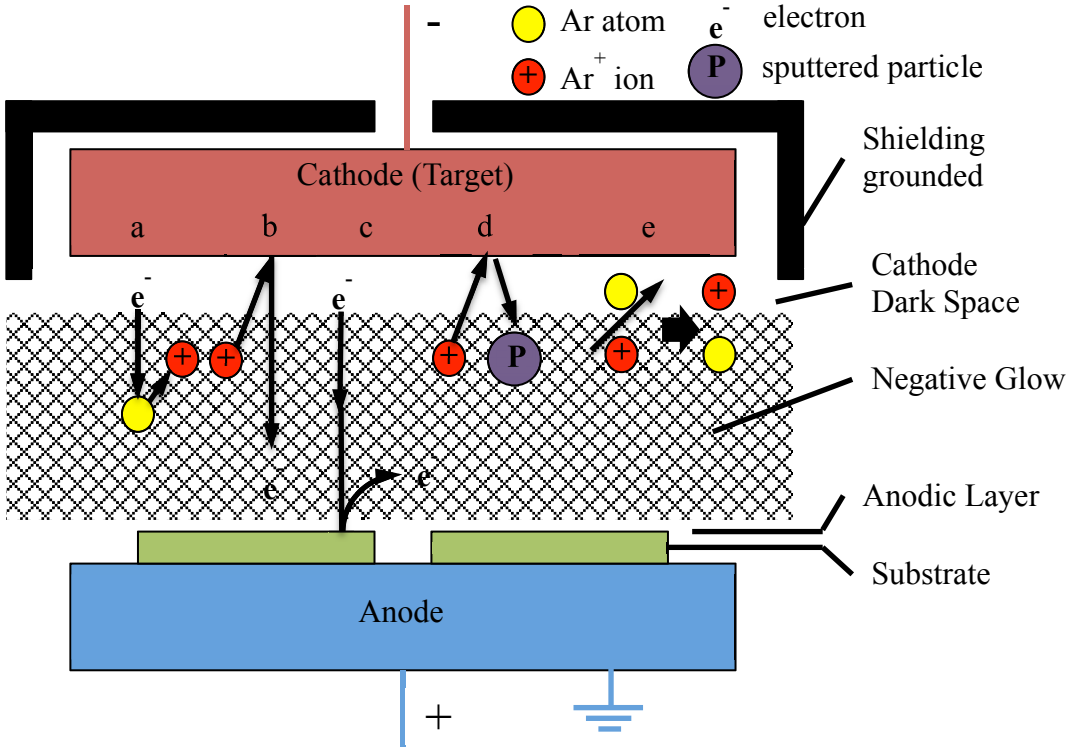

Figure 2.2: Particle interactions occurring during the sputter process [20]. (a) an electron ionizes an atom, (b) ion induced electron emission, (c) electron induced emission of secondary electrons from the anode, (d) sputtering caused by accelerated ion, (e) symmetric charge exchange.

In general, sputtering is the physical vaporization of atoms from a liquid or solid material. Due to the bombardment of high energetic particles (mostly ions), which are accelerated towards the target by applying a negative voltage at the cathode, the atoms close to the surface of the target can be vaporized. These collisions indicate a transfer of energy from the ions to the target atoms causing collision cascade and a transfer of momentum. However, to sputter an atom from the target, its binding energy has to be overcome, leading to a direct proportional relationship between the sputter yield and the ion energy. Furthermore the sputter yield also depends on the mass of the target atom, the mass of the ion and its angle of incidence [18–21].

2.1.2 Reactive and non-reactive sputtering

Non-reactive sputtering without using a reactive gas like N_2 or O_2 is performed to sputter compounds, alloys or metals. However differences in the element masses of the alloys and sputter yields may result in a different chemical composition of the film to the target material. Compounds are sputtered as molecule as well as fragments of it i.e. an oxide mainly vaporizes in form of a metal, a metal oxide and oxygen. Further on, some compounds like TiO_2 indicate decreased sputter yields due to the strong ionic binding character. Generally, the thermal and electrical conductivity have to be considered of such compound or alloyed targets to choose the correct powering of the target [19,21].

The use of a reactive working gas during sputtering enables depositing coatings with defined stoichiometry and chemical composition, by simply varying the reactive gas partial pressure. For example when reactively sputtering Cr in different N_2 containing atmospheres, i.e., different N_2/Ar ratios, either CrN or Cr_2N can be prepared [22]. The randomly moving particles within a plasma can react in three different ways: 1) forming molecules at the target surface, 2) forming molecules with sputtered atoms from the target in the gas phase and 3) adsorption of the gas atoms at the substrate surface to form molecules with the sputtered target material [20]. The remained molecules at the target surface decrease the sputter yield, especially when forming a non-conductive layer on the target. This effect is well known as target poisoning. Therefore it is necessary to adjust the process parameters, to achieve an acceptable sputter yield combined with the desired chemical composition and stoichiometry of the coating material [20,21].

2.2 Film formation

2.2.1 Nucleation and film growth

The nucleation process ranges from the formation of a nucleus of critical size to the crystal growth as schematically shown in Figure 2.3. The process start is indicated by the transport of a vaporized particle from the target through the plasma and the condensation at the substrate surface. This particle can re-evaporate immediately or become thermally accommodated. The

formation of a metastable cluster correlates with the mobility of the atoms, which depends on the ratio of the substrate temperature to the melting point (T_S/T_M), the homologous temperature. At high temperatures a metastable cluster can be formed as the diffusivity and consequently the mobility of the accommodated particles is high enough. However the clusters grow and coalesce with neighboured clusters in order to reduce the total surface energy. As low temperatures correspond with low mobility of the atoms, the atoms tend to arrange randomly leading to amorphous structured coatings. These early stages of the film growth determine the first atomic layers of the film and influence the adhesion of the film and the morphology on the substrate [19,21,23].

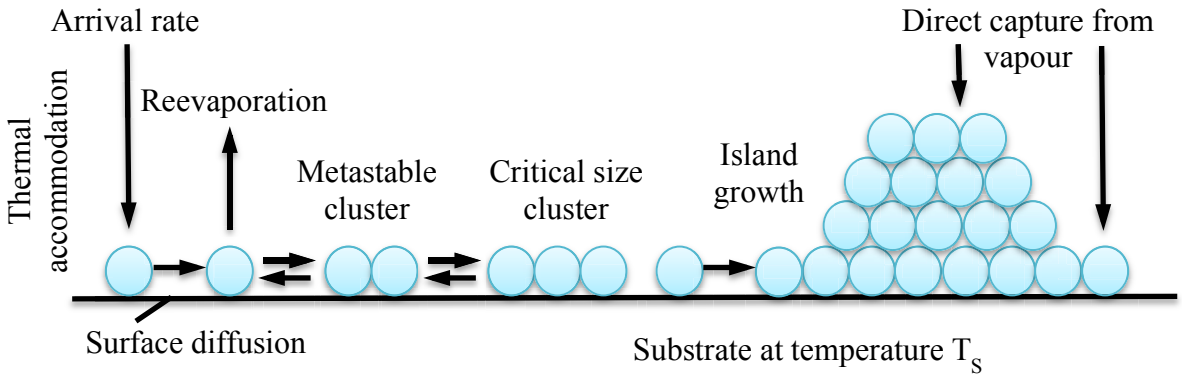

Figure 2.3: Formation and growth of a nucleus [19,24].

After the nucleation, the continuous growth of crystals with different crystal orientations is initiated. As crystal orientations with low surface energy are favoured during the film growth, grains tend to grow up in these crystal orientations to keep the surface energy as low as possible in the coating. Moreover the film growth also depends on the roughness of the substrate surface, the diffusion of the condensed atoms and the binding energy between the substrate and the film. Figure 2.4 illustrates schematically the three modes of nucleation and film growth. Typical sputtered films are indicated by 3-D island structures (Volmer-Weber-growth, see Figure 2.4 (a)) as the atoms exhibit higher binding energy to each other than to the substrate. This model is based on stable clusters, which grow in form of islands and coalesce. The model of Frank-van der Merwe (see Figure 2.4 (b)) represents a 2-D layer-by-layer growth, where the binding energy of the atoms is equal, or less between the atom and the substrate. The third model was predicted by Stranski-Krastanow (see Figure 2.4 (c)), which is a combination of Volmer-Weber and Frank-van der Merwe. Here the growth process

starts with the 2-D layer-by-layer growth and after one or more monolayers the 3-D island growth develops [18,19].

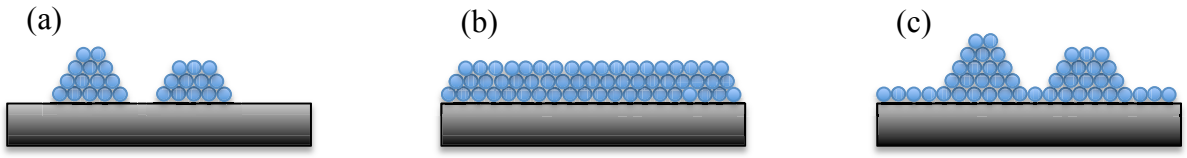

Figure 2.4: Nucleation modes [23]. (a) island growth (Volmer-Weber), (b) 2D layer by layer growth (Frank-van der Merwe), (c) layer and island growth (Stranski-Krastanow).

2.2.2 Structure zone models

There are a lot of parameters such as substrate temperature, bias voltage and gas pressure influencing the film growth and the coating morphology. Figure 2.5 shows the results of the studies on these parameters examined by Thornton [25] and Messier [26]. The graph of Thornton's model (see Figure 2.5 (a)) represents the obtained coatings morphology as function of the working pressure of Ar and the ratio of substrate temperature (T_S) with respect to the melting point (T_M). Additionally, Messier investigated the influence of kinetic energy by variations of Bias voltage on the structural development of the formed coatings.

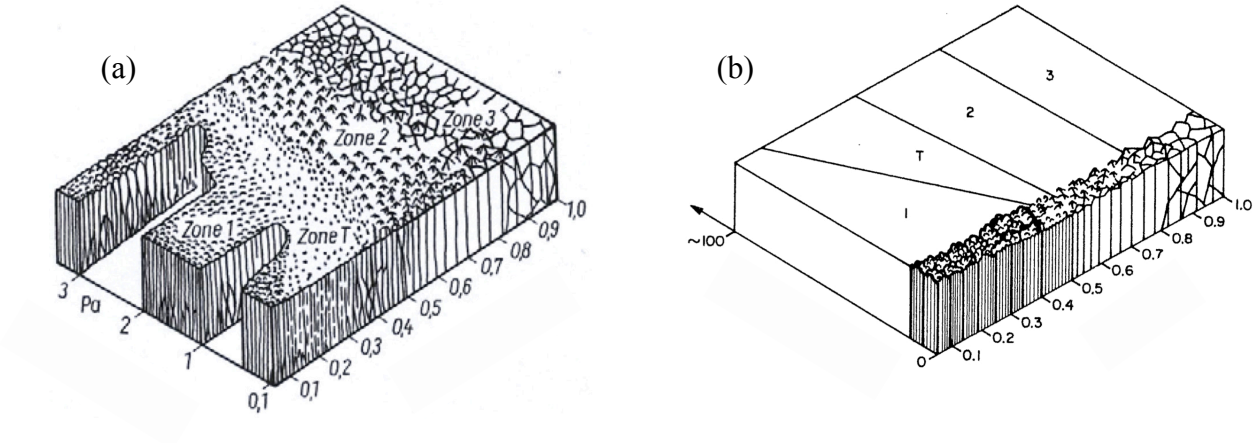

Figure 2.5: Structure zone models of (a) Thornton [25] and (b) Messier [26].

Zone I ($T_S/T_M \leq 0.1$) represents columnar, porous structured films with low density due to low adatom mobility and low temperatures.

Increasing the temperature, hence increasing T_S/T_M, which corresponds to an increased mobility of the adatoms, results in films with dense columnar structure. This is characterized by Zone T ($0.1 < T_S/T_M \leq 0.3$), which is the transition zone between Zone I and Zone II.

A further increase of the substrate temperature enables grain boundary motion and growth of coarser grains due to the already possible volume-diffusion. In contrast to the transition zone the obtained coating morphology in Zone II ($0.3 < T_S/T_M \leq 0.5$) shows coarse columns.

Homologous temperatures > 0.5 (Zone III) allows for recrystallization and volume diffusion as well as bulk diffusion resulting in dense structured coatings with large equiaxed grains and a smooth surface [25].

In contrast to Thornton, who investigated the coating morphology in dependence on the homologous temperature and the working gas pressure, Messier additionally investigated the influence of different bias voltages applied to the substrate, as presented in Figure 2.6 (b). The graph represents, that with increasing bias voltage Zone T expands to lower homologous temperatures due to higher energy of the incident particles. This is particularly interesting for sputtering at low temperatures as also dense fibrous grains can grow just by increasing the bias voltage [26].

3 Coating system

Transition metal nitrides like CrN and TiN are commonly used in industry to protect the surface against corrosion, oxidation, abrasive or thermal loads, for cutting, milling and forming applications. Adding AlN within these coatings to form either a ternary monolithically grown material or multilayer coatings result in a further improvement of their properties. Especially the CrN/AlN multilayer architecture demonstrates promising results for hard and wear protective coatings [12,27–29].

3.1 Chromium nitride – CrN

The phase diagram of Cr-N (see Figure 3.1) shows two phase modifications in the solid state (hexagonal Cr_2N and cubic or orthogonal CrN). Paramagnetic CrN stabilizes in the face-centred cubic (c-) structure above the Nèel temperature in the range of 273 – 283 K [30]. The schematic in Fig. 3.2 shows the c-structure of CrN with the N atoms at the octahedral sites (grey balls) and the Cr atoms at the corners and the centre of the faces (blue balls). This fcc structure exists in a very narrow range extending from 49.5 to 50.0 at. % N and therefore depends on the nitrogen partial pressure used during deposition. c-CrN is thermally stable up to approximately 1000 °C measured at atmospheric pressure [30,31]. Increasing the annealing temperature results in decomposition of CrN to form Cr_2N and released N_2. The formed Cr_2N than further dissociates to (body centred cubic, bcc) Cr and N_2 if the temperature is increased further [30,32].

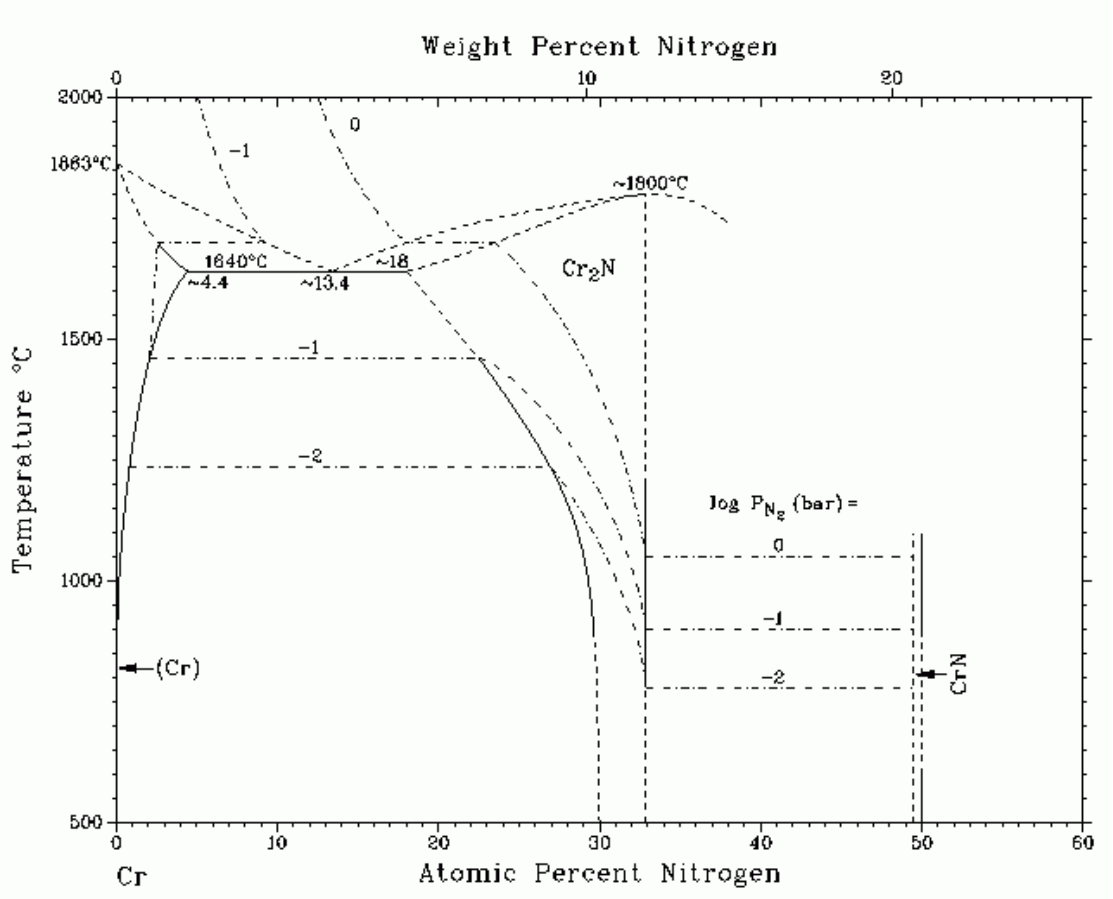

Figure 3.1: Binary phase diagram Cr-N [33].

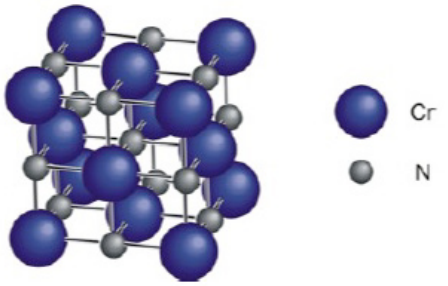

Figure 3.2: Crystal structure of CrN: NaCl (B1) structure [34].

CrN hard coatings have a comparable microhardness to TiN hard coatings and are one of the most used transition metal nitrides since the 1980's [35]. Further reasons to deposit CrN on a substrate are its excellent oxidation and corrosion resistance and higher fracture toughness [36,37].

3.2 Aluminium nitride – AlN

In contrast to CrN, AlN has a hexagonal close packed ZnS-wurtzite-type (w-) structure (see Figure 3.3 (a)). This structure is thermally stable up to ~2800 °C. The w-AlN structure has a wide band gap and therefore it is mainly used as semiconductor material in ultraviolet optoelectronic applications, as mainly covalent and ionic bindings are present without metallic character [38]. Typical hardness values are in the range of ~14 – 20 GPa and due to the missing metallic bindings a more brittle fracture behaviour is present when compared to c-CrN [39,40]. However a metastable face centred cubic NaCl-structure of AlN (see Figure 3.2. (b)) can be stabilized under high-pressure or if the layer thickness of AlN is below ~3.3 nm when preparing superlattice coatings either in combination with TiN or CrN [41–43]. The hardness of c-AlN is in the range of ~39 – 49 GPa [44]. These cubic modifications of AlN and CrN are needed to fulfil the requirements of preparing single-phase cubic structured CrN/AlN superlattice coatings, guaranteed by an epitaxial growth of the individual layers.

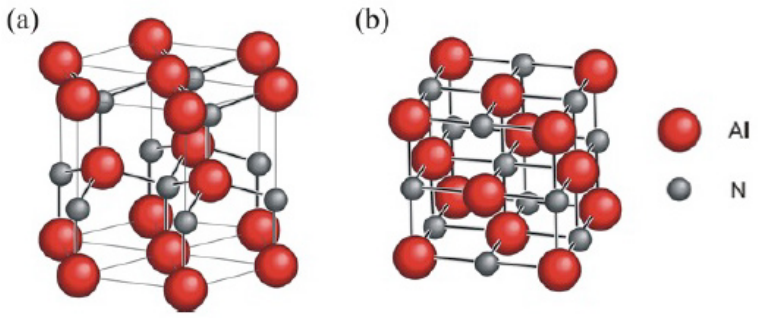

Figure 3.3: Possible lattice structures of AlN in this study: a) thermally stable ZnS w-structure and b) metastable NaCl c-structure [34].

3.3 Multilayer coatings

Multilayer coatings showed advanced properties for cutting and milling tools regarding their lifetime. These coatings are indicated by alternatingly grown layers and extend the field of application compared to monolithically grown coatings. The properties of the coatings like hardness, toughness, oxidation and corrosion resistance can be adjusted by their bilayer period Λ and hence the number of interfaces. The latter becomes more important especially for the mechanical properties as well as fracture toughness as the crack-propagation can be influenced. Furthermore, the layered architecture can also stabilize the crystal structure of

individual layers in a specific metastable one by the effect of coherency strains to the other layers. In the past 10 years the individual layer thickness within the coating was downsized to a few nm resulting in a small Λ. This class of coatings are called superlattice coatings which are often represented by increased mechanical and thermal properties [45–49].

3.4 Superlattice coatings

Superlattice coatings are multi-layered coatings composed of layers having the same crystal structure and similar lattice parameters. Generally, the individual layer thicknesses are in the range of some few nm, and by the alternating arrangement of individual layers with the same crystal structure so-called superlattices can form. The layers do not need to have the same crystal structure, as strain-induced stabilization can help to allow for an epitaxial growth of the individual layers as well [50]. Very often, such superlattices exhibit increased hardness values, thermal resistance and wear protection when compared to their individual constituents. The inherent sharp interfaces between the individual layers of such superlattices act as obstacles for dislocation motion and glide resulting in an increased hardness as well as oxidation and corrosion resistance [12,27,28]. Different effects, as described in more detail in the following paragraphs, are responsible for their properties.

As mentioned above, the template effect (strain-induced stabilization) in superlattice coatings allows combining normally non-isostructural materials (both layer-materials do not exhibit the same crystal structure). A layer can crystallize in a metastable phase having the same crystal structure as the layer it grows onto. This so-called “template effect”, as it is the result of a strain-effect to the template-layer, is of course decreasing with increasing thickness of the growing layer (and hence to the interface). Within this work the effect of stabilizing the usually wurtzite AlN in its metastable cubic structure by the use of a cubic CrN template-layer is investigated in detail. Literature reports, that the AlN layers can be stabilized in their cubic structure up to layer thickness of 3.3 nm, when grown on cubic CrN, which leads to the formation of the superlattice CrN/AlN coatings [41].

Yashar et al. [51] described that different strengthening mechanisms are responsible for the observed hardness increase when preparing superlattice coatings. These include the Hall-Petch effect, the mechanism of image forces on dislocations at the interfaces, the dislocation movement in an alternating strain filed and the supermodulus effect. The latter was detected

during early experiments on metallic multilayer coatings and showed improvements of their elastic properties by about 100% as compared to their constituent layers [51].

The first attempt to describe the hardening effect of superlattice coatings was conducted by Koehler [52]. Koehler noted that the layers should be thin enough to avoid dislocation generation within the layers. This theory is based on hindering the dislocation motion in a superlattice coating leading to high hardness. The reasons for this increase in hardness are different dislocation line energies of each layer having different shear moduli and image forces influencing the dislocations. Due to this a certain shear stress is required, if a dislocation is crossing an interface and moves from the layer with lower shear modulus into the layer with higher shear modulus. The stress depends further on the crystallographic orientation of the multilayer coating, the number of interfaces, the individual layer thicknesses and the angle between the dislocations glide plane and the interface. If the bilayer period becomes extremely thin the required shear stress decreases due to an increased contribution from other interfaces of the multilayer coating. Another factor concerning the image forces is that the interfaces of a real multilayer are not ideally sharp. This results in an increase of the interface widths and decreases the required shear stress to move the dislocation across the interface. Hence, dislocations can be generated and are able to move within thick layers without encountering an interface.

A good approach for the hardness-profile of superlattice coatings is given by the Hall-Petch effect, which describes mechanical properties of polycrystalline materials with respect to their grain size as follows [53]:

$$H = H_0 + kD^{-1/2}, \tag{1}$$

where H is the resulting hardness, D is the grain size, H_0 is the hardness of the material with large grains and k is a material constant. The model of polycrystalline bulk materials is based on the theory that dislocations cannot move through grain boundaries and dislocation pile-ups in one grain have to initiate a dislocation source in a neighboured grain [53]. This model is transferred to multilayer systems replacing the grain size with the bilayer period. The individual layers act as grains with additional grain boundaries (i.e., layer boundaries or interfaces between the individual layers). Furthermore, multilayer coatings having a bilayer

period below 20 nm require an extended Hall-Petch model, which takes the very thin individual layer thicknesses into account. Therefore, the model has been modified by Anderson et al. [54], considering the effect of lattice mismatch between the layers and lattice slip planes, the number of dislocation loops, image forces on dislocations, structural differences and differences in stacking fault energy. Moreover, this extended model focuses especially on the influence of misfit dislocations on the hardening effect. Applying this model on multilayer coatings with bilayer periods larger than 100 nm a H vs. $\Lambda^{-1/2}$ behaviour as the basic Hall-Petch equation predicts can be observed [54]. Below this bilayer period the profile of hardness reaches a maximum at the point where only space for one dislocation is left in the individual layers. Basically the model gives an overview of the dependence of the hardness on Λ as schematically shown in Figure 3.4 [50–52,55–59].

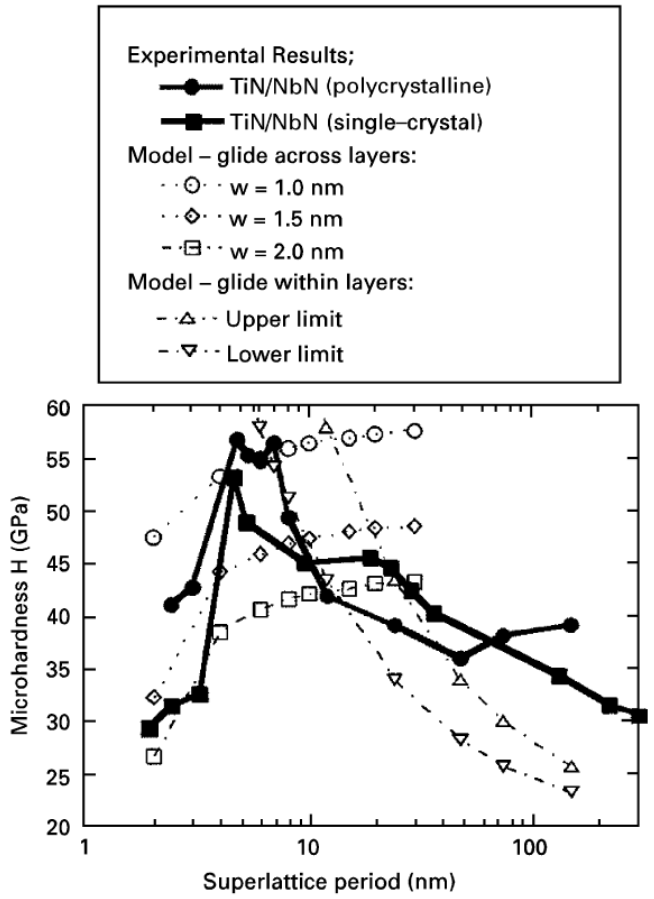

Figure 3.4: Hardness vs. Λ profiles of experimental and model data in comparison for single and polycrystalline TiN/NbN multilayers [60].

4 Characterization Techniques

4.1 X-ray diffraction

Scattering techniques are widely used to investigate the crystal structure of materials in research. X-ray diffraction is a non-destructive investigation method to determine the crystal structure of solids. Since the small bilayer periods of the CrN/AlN superlattice coatings can be measured with less effort as compared to high-resolution transmission electron microscopy (HRTEM) investigations by low and high angle X-ray diffraction mode (LAXRD and HAXRD), the following chapter focuses on these topics of X-ray diffraction in more detail.

4.1.1 Low angle X-ray diffraction – LAXRD

LAXRD (for $2\theta \leq 15$ °) can be used to non-destructively and fast determine the bilayer period of multilayer coatings from the angular position of the peaks in the pattern. The effects are based on X-ray reflectivity (XRR), where the peak formation results from the interference of the waves reflected from individual (e.g., the interface above and below a certain layer) interfaces of the layers as schematically shown in Figure 4.1. This interference effect substantially depends on differences in electron density and refractive indices and the interface roughness. Such an interface acts like a “semi-transparent mirror”, transmitting or reflecting the incident beam, if the absorption of the beam in a layer is not too high. In case of reflection, the intensity of the reflected beam is influenced by the individual layer thickness and the sum-curve of the individual maxima is related to the structure factor of the multilayer coating. In 1954 L.G. Parratt [61] was the first researcher, who published a paper concerning the reflectivity of a substrate, which is covered with numerous layers having distinct electron densities and absorption coefficients. The formalism considers the reflection of each layer and the phase difference of the reflected beams from different layers. [61,62].

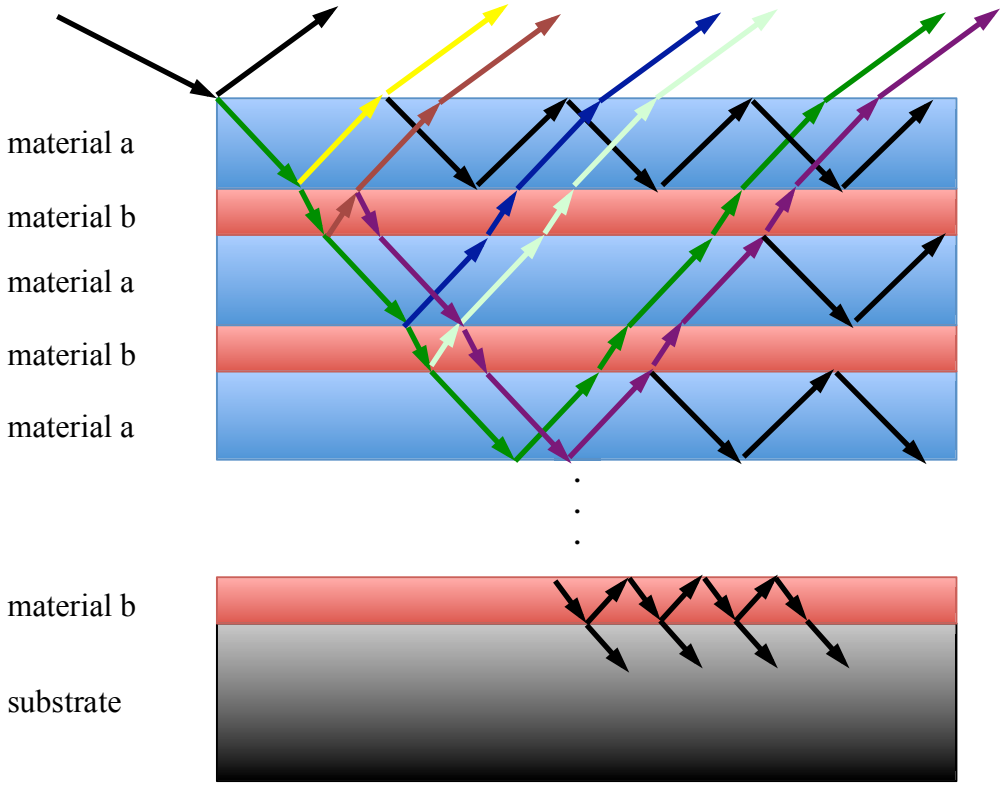

Figure 4.1: Scheme of transmitted and reflected beams in a multilayer, adapted from [63].

Examples of LAXRD patterns of CrN/AlN superlattice coatings prepared within this thesis are given in Figure 4.2. The order of the peaks ranges from first to third (m = 1, 2 and 3).

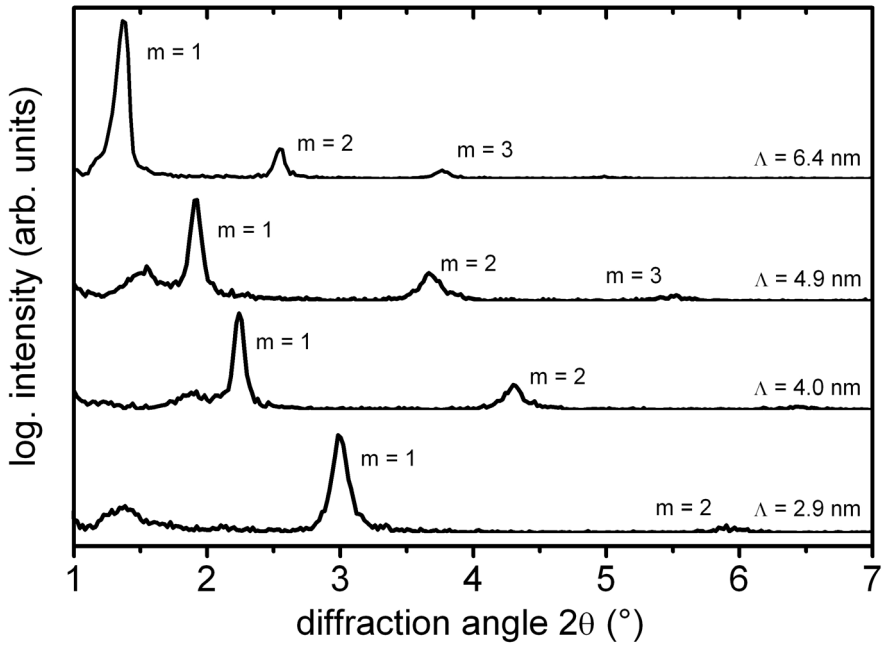

Figure 4.2: LAXRD patterns of CrN/AlN multilayer coatings composed of 1 nm thin AlN layers with bilayer periods Λ from 2.9 nm to 6.4 nm.

The bilayer period can be calculated with the peak positions using the modified Bragg equation [51]:

$$\Lambda = \frac{m\lambda}{2\sin(\theta)}, \tag{2}$$

where m is the order of the reflection peak in the LAXRD pattern, λ, the wavelength of the X-ray beam, θ, is half of the Bragg diffraction angle and Λ is the bilayer period [51,62,64,65]. Table 1 gives the settings used for the LAXRD measurements in this study:

Table 1: LAXRD parameters used for the characterization of the CrN/AlN multilayers

- Method: gracing incident
- Incident angle: 1°
- 2θ range: 0.5 – 7°
- Stepsize: 0.02 °
- Steptime: 2.4 s
- Slit: 0.1 or 0.3°
- Cu K_α tube voltage: 20 kV
- Cu K_α tube current: 5 mA

4.1.2 High angle X-ray diffraction – HAXRD

The θ-2θ geometry (Bragg-Brentano) is generally used for HAXRD experiments (2θ > 15°). It has to be taken into account, that a HAXRD pattern is a combination of the variation of the lattice spacing and the chemical composition. The diffraction patterns of our single-phase cubic superlattice coatings reveal a periodic sequence of satellite peaks next to the diffraction peaks. The position of these satellite peaks depends on the thickness of the individual layers and the lattice mismatch at the interface. Defects and rough (not ideal sharp) interfaces smear the satellite peaks and the peaks with higher order (m > 2) cannot be detected anymore.

Figure 4.3 shows HAXRD patterns from CrN/AlN superlattice coatings prepared within this thesis indicating the (111) Bragg peak flanked by satellite peaks on the left side at smaller diffraction angles, which are of the -1st order (m = -1). These satellite peaks indicate the superlattice structure as they shift from the main XRD peak to higher diffraction angles with increasing Λ.

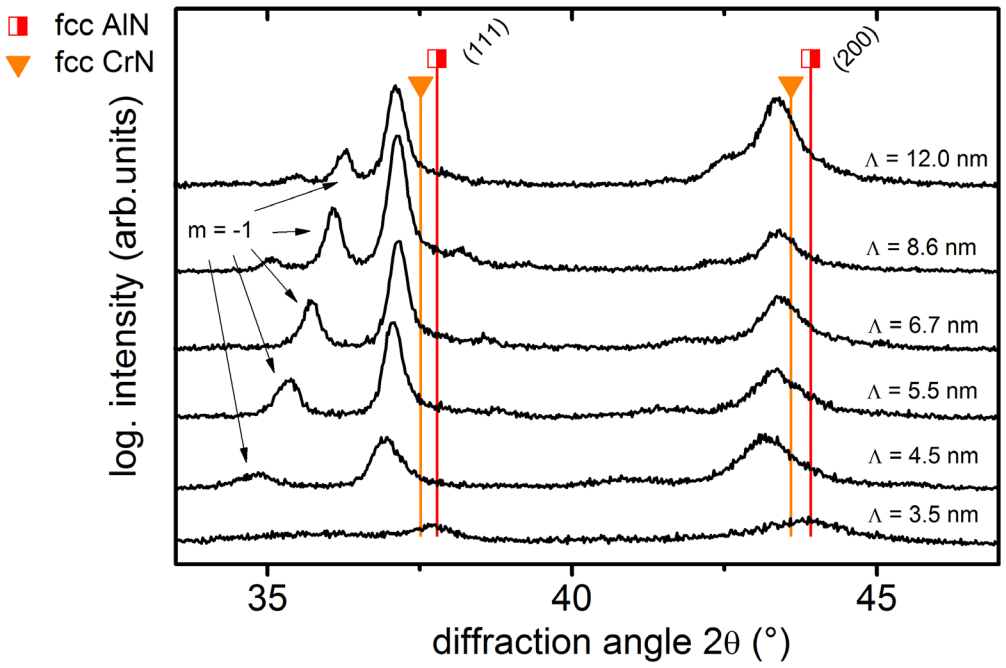

Figure 4.3: HAXRD pattern from CrN/AlN multilayers composed of 2 nm thin AlN layers with bilayer periods from 3.5 to 12 nm.

Similar to LAXRD the bilayer period can be calculated by the peak positions of the main Bragg peak and the satellite peaks. The modified Bragg relation is given by [51]:

$$sin\theta_{\pm} = sin\theta_B \pm \frac{m\lambda}{2\Lambda}, \tag{3}$$

where m is the order of the satellite peak, λ, the wavelength of the X-ray beam, θ_B, half of diffraction angle of the main Bragg peak, $\theta_{\pm}$, half of the angle position of the satellite peak and Λ is the resulting bilayer period. Table 2 shows the settings used for the HAXRD measurements:

Table 2: HAXRD parameters used for the characterization of the CrN/AlN multilayers

- Method: Bragg Brentano
- 2θ range: 30-85°
- Stepsize: 0.02°
- Steptime: 1.2 s
- Slit: 1.0°
- Cu K_α tube voltage: 40 kV
- Cu K_α tube current: 25 mA

Both investigation methods have their advantages and disadvantages. LAXRD is a very fast method to determine mainly the bilayer period. HAXRD experiments need more time, but the resulting patterns give also information on the crystal structure, lattice plane distances for certain crystallographic orientations, micro- and macro-strains as well as the bilayer period by means of the satellite peak position [48,51,62].

4.2 Transmission electron microscopy (TEM)

To investigate the crystal structure of a solid in more detail, rays with smaller wavelength and higher energy than those of X-rays are needed. This enables investigations on the nanometre scale and allows imaging of e.g., precipitations or individual layers in the range a few nm. The principle of a TEM is based on thermally emitted and accelerated electrons, which transmit through a nm-thin sample. The electron wave passes some electromagnetic lenses before it is diffracted and scattered forward by the sample. One of these lenses, the objective lens, is the limiting factor of the optical resolution of a TEM. The imaging of a TEM depends mainly on the used apertures and configuration of the lenses. The operation modes are bright and dark field imaging, diffraction as well as lattice imaging. Different possibilities are known to improve the quality and avoid aberrations of the obtained TEM image, but the best images are taken with best prepared specimen [66].

4.3 Nanoindentation

A UMIS Nanoindenter from the Fischer-Cripps Laboratories equipped with a Berkovich tip was used to measure the hardness of the CrN/AlN superlattice coatings within this thesis. Popular methods e.g., Vickers or Brinell, use different indenter tips and determine the projected area of the remaining imprint of the indentation to calculate the hardness of the solid. Consequtently the hardness depends on the applied load (P) and the remaining size of the projected area (A) as follows:

$$H = \frac{P}{A} \tag{4}$$

This method is especially for thin films with small loads and indentation depths (hence a small remaining indent) not applicable. A generally accepted requirement to minimize the substrate-interference for the hardness measurements of thin films is, that the indentation depth is below 10% of the coating thickness. As a rule of thumb for ~3 µm thin coatings this would leave an indent with a lateral edge of the projected area of only ~1 µm. Consequently, computer controlled nanoindenters are used to determine the hardness of such films. During the loading/unloading procedure of the UMIS Nanoindenter a load-displacement curve is recorded. Out of this curve the hardness and the Young's modulus can be calculated by the method of Oliver and Pharr [67]. The effects of elastic and plastic deformation during the loading and unloading are taken into account by this method. The obtained values by this method have to be critically reviewed as the quality of the surface of the films or vibrations influence the test procedure as well as the sensitivity of the measurement arrangement [68,69].

4.4 Biaxial stress measurement

The residual stresses of a specimen (substrate-coating composite) are resulting from intrinsic (nucleation and growth) and extrinsic (thermal) stresses. These stresses lead to a loss of adhesion, film cracking and film yielding. Further, the stresses of the coating drive the coating-substrate composite to curl. This bending is measureable by two parallel laser beams, which hit the surface and reflect in a corresponding angle to the curvature. The stresses within this work were measured a measurement arrangement schematically shown in Fig. 4.4, for more details on the measuring principle, see [24].

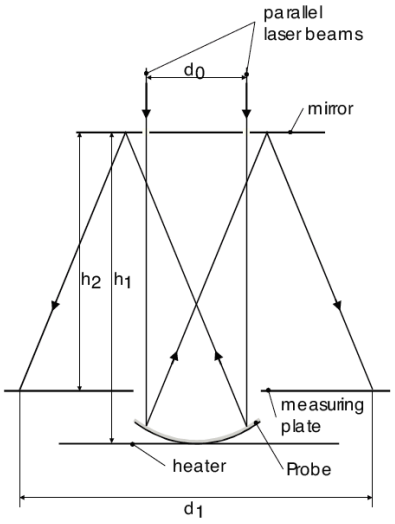

Figure 4.4: Laser beam path of the biaxial stress measurement arrangement [24]

5 Deposition system

The CrN/AlN multilayer coatings were prepared in an Ar/N_2 glow discharge using an AJA Orion 5 lab-scaled deposition plant shown in Figure 5.1 a).

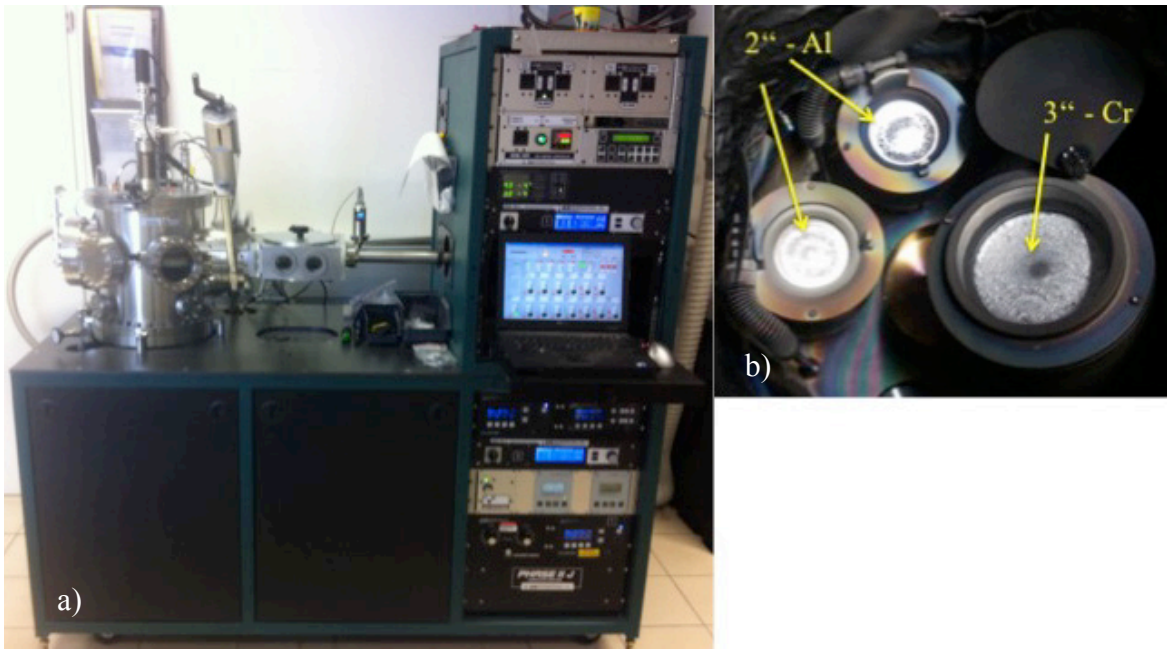

Figure 5.1: a) Orion 5 - lab-scaled PVD System with computer-controlled shutter system from AJA b) Positioning of the Cr and Al targets in the vacuum chamber.

A computer controller allows for preparing multilayer coatings with a defined bilayer period by either sequentially switching on and off the guns or using the shutter system. Within this work two 2'' Al targets and one 3'' Cr target, positioned as shown in Fig. 5.1b, were used. The N_2 partial pressure was adjusted to 240 mPa by using an N_2 flow rate o 6 sccm and an Ar flow rate of 4 sccm to allow for the preparation of stoichiometric cubic CrN. Moreover, RF – substrate biasing of -70 V was used to assure dense multilayer coatings and the substrates were heated to 470 °C. The CrN/AlN superlattice coatings were deposited with parameters as listed in Table 3:

Table 3: Deposition parameters used for the preparation of the CrN/AlN multilayers

- Substratre rotation: 60 rpm
- Substratet temperature: 470 °C
- Total pressure: 400 mPa
- Ar flow: 4 sccm
- N_2 flow: 6 sccm

6 Bibliography

[1] M. Ohring, Material Science of Thin Films, 2nd ed., Academic Press, 2001.

[2] M. Riehle, E. Simmchen, Grundlagen Der Werkstofftechnik, Wiley, 2001.

[3] G.S. Fox-Rabinovich, B.D. Beake, J.L. Endrino, S.C. Veldhuis, R. Parkinson, L.S. Shuster, M.S. Migranov, Surface and Coatings Technology 200 (2006) 5738–5742.

[4] G. a. Zhang, P.X. Yan, P. Wang, Y.M. Chen, J.Y. Zhang, Materials Science and Engineering: A 460-461 (2007) 301–305.

[5] Z. Han, J. Tian, Q. Lai, X. Yu, G. Li, Surface and Coatings Technology 162 (2003) 189–193.

[6] S.-Y. Yoon, K.O. Lee, S.S. Kang, K.H. Kim, Journal of Materials Processing Technology 130-131 (2002) 260–265.

[7] W.-J. Chou, G.-P. Yu, J.-H. Huang, Surface and Coatings Technology 149 (2002) 7–13.

[8] R. Rachbauer, D. Holec, P.H. Mayrhofer, Surface and Coatings Technology (2011).

[9] R. Rachbauer, D. Holec, M. Lattemann, L. Hultman, P.H. Mayrhofer, International Journal of Materials Research (formerly Zeitschrift Fuer Metallkunde) 102 (2011) 735–742.

[10] C. Chen, J. Pascual, F. Fischer, O. Kolednik, R. Danzer, Acta Materialia 55 (2007) 409–421.

[11] S. Zhang, J. Li, Z. Chen, M. Li, Thin Solid Films 520 (2012) 4984–4989.

[12] J. Lin, J.J. Moore, B. Mishra, M. Pinkas, X. Zhang, W.D. Sproul, Thin Solid Films 517 (2009) 5798–5804.

[13] L. Hultman, C. Engström, M. Odén, Surface and Coatings Technology 133-134 (2000) 227–233.

[14] X.T. Zeng, Surface and Coatings Technology 113 (1999) 75–79.

[15] A. Thobor, C. Rousselot, C. Clement, J. Takadoum, N. Martin, R. Sanjines, F. Levy, Surface and Coatings Technology 124 (2000) 210–221.

[16] D.C. Cameron, R. Aimo, Z.H. Wang, K.A. Pischow, Surface and Coatings Technology (2001) 567–572.

[17] K. Choy, Progress in Materials Science 48 (2003) 57–170.

[18] P.M. Martin, Handbook of Deposition Technologies for Films and Coatings, 3rd ed., Elsevier Inc., 2010.

[19] D.M. Mattox, Handbook of Physical Vapor Deposition (PVD) Processing Film Formation, Adhesion, Surface Preparation and Contamination Control, Noyes Publications, 1998.

[20] R.A. Haefer, Oberflächen- Und Dünnschicht-Technologie, Springer-Verlag, Berlin, 1987.

[21] W.D. Westwood, Sputter Deposition, AVS, New York, 2003.

[22] P.H. Mayrhofer, G. Tischler, C. Mitterer, (2001) 78–84.

[23] P.B. Barna, M. Adamik, Thin Solid Films 317 (1998) 27–33.

[24] P.H. Mayrhofer, Materials Science Aspects of Nanocrystalline PVD Hard Coatings, Montanuniversität Leoben, 2001.

[25] J.A. Thornton, Journal of Vacuum Science and Technology 11 (1974) 666.

[26] R. Messier, A.P. Giri, R.A. Roy, Journal of Vacuum Science & Technology A: Vacuum, Surfaces, and Films 2 (1984) 500–503.

[27] J.-K. Park, Y.-J. Baik, Surface and Coatings Technology 200 (2005) 1519–1523.

[28] J. Lin, J.J. Moore, J. Wang, W.D. Sproul, Thin Solid Films 519 (2011) 2402–2408.

[29] G.S. Kim, S.Y. Lee, J.H. Hahn, Surface and Coatings Technology 171 (2002) 91–95.

[30] P.H. Mayrhofer, F. Rovere, M. Moser, C. Strondl, R. Tietema, Scripta Materialia 57 (2007) 249–252.

[31] P.H. Mayrhofer, H. Willmann, a. E. Reiter, Surface and Coatings Technology 202 (2008) 4935–4938.

[32] M.-A. G.Djouadi, C. Noveau, O. Banakh, R. Sanjines, F. Levy, G. Nouet, 152 (2002) 510–514.

[33] J.M. Venkatraman, J.P. Neumann, Binary Alloys Phase Diagrams 1 (1990).

[34] H. Willmann, Al-Cr-N Thin Film Design for High Temperature Applications, Montanuniversity of Leoben, 2007.

[35] L. Cunha, M. Andritschky, Surface and Coatings Technology 111 (1999) 158–162.

[36] M. Berger, R. Westergard, T. Bjork, S. Hogmark, J. Bergstrom, 147 (2001) 33–41.

[37] P.H. Mayrhofer, H. Willmann, C. Mitterer, 147 (2001) 222–228.

[38] http://www.ioffe.ru/SVA/NSM/Semicond/AlN/index.html, Ioffe Physico-Technical Institute (2012).

[39] P.H. Mayrhofer, D. Music, J.M. Schneider, Applied Phys. Let. 88 (2006) 071922.

[40] S.-R. Jian, G.-J. Chen, J.S.-C. Jang, Y.-S. Lai, Journal of Alloys and Compounds 494 (2010) 219–222.

[41] J. Lin, J.J. Moore, B. Mishra, M. Pinkas, W.D. Sproul, Surface and Coatings Technology 204 (2009) 936–940.

[42] N.E. Christensen, I. Gorczyca, Phys. Rev. 50 (1994) 4397.

[43] I. Petrov, E. Mojab, R.C. Powell, J.E. Greene, L. Hultman, J.E. Sundgren, Appl. Phys. Lett. 60 (1992) 2491.

[44] J. Zhu, D. Zhao, W.B. Luo, Y. Zhang, Y.R. Li, Journal of Crystal Growth 310 (2008) 731–737.

[45] W.D. Sproul, Surface and Coatings Technology 86-87 (1996) 170–176.

[46] H. Jensen, J. Sobota, G. Sorensen, Surface and Coatings Technology 94-95 (1997) 174–178.

[47] H. Jensen, G. Sorensen, I. Mannike, F. Muktepavela, J. Sobota, Surface and Coatings Technology 116-119 (1999) 1070–1075.

[48] C.J. Tavares, L. Rebouta, B. Almeida, J. Bessa e Sousa, Surface and Coatings Technology 100-101 (1998) 65–71.

[49] M. Larsson, P. Hollman, P. Hedenqvist, S. Hogmark, U. Wahlström, L. Hultman, Surface and Coatings Technology 86-87 (1996) 351–356.

[50] M. Setoyama, A. Nakayama, M. Tanaka, N. Kitagawa, T. Nomura, Surface and Coatings Technology 86-87 (1996) 225–230.

[51] P.C. Yashar, W.D. Sproul, Materials Science 55 (1999) 179–190.

[52] K. J.S., Physical Review 2 (1970) 547–551.

[53] E. Hall, Proc Phys Soc London 64B (1951) 747.

[54] P.M. Anderson, C. Li, 5 (1995) 349–362.

[55] K. J.S., Physical Review 86 (1952) 52 – 59.

[56] S. Veprek, Surface and Coatings Technology 97 (1997) 15–22.

[57] S. Veprek, R.F. Zhang, M.G.J. Veprek-Heijman, S.H. Sheng, a. S. Argon, Surface and Coatings Technology 204 (2010) 1898–1906.

[58] M.-S. Wong, G. Hsiao, S. Yang, (2000) 160–165.

[59] F.H. Mei, N. Shao, J.W. Dai, G.Y. Li, Materials Letters 58 (2004) 3477–3480.

[60] X. Chu, S. Barnett, Appl Phys 77 (1995) 4403.

[61] L.G. Parratt, E.L. Jossem, Physica 20 (1954) 1134–1137.

[62] V. Holy, U. Pietsch, T. Baumbach, High-Resolution X-ray Scattering from Thin Films and Multilayers, Springer, 1999.

[63] O. Werzer, Reflectivity, TU Graz, 2007.

[64] H. Vanderstraeten, D. Neerinck, K. Temst, Y. Bruynseraede, E.E. Fullerton, I.K. Schuller, Journal of Applied Crystallography 24 (1991) 571–575.

[65] Mario Birkholz, Thin Film Analysis by X-Ray Scattering, WILEY-VCH, 2006.

[66] D.B. Williams, C.B. Carter, Transmission Electron Microscopy, 2nd ed., Springer, 2009.

[67] W.C. Oliver, G.M. Pharr, (1992).

[68] A.C. Fischer-Cripps, Surface and Coatings Technology 200 (2006) 4153–4165.

[69] S. HAN, R. SAHA, W. NIX, Acta Materialia 54 (2006) 1571–1581.

7 Publication

Influence of the bilayer period on the structure of AlN and the mechanical properties of CrN/AlN superlattice coatings

B. Mayer, M. Schlögl, J. Paulitsch, P.H. Mayrhofer

Manuscript in final preparation

Introduction

In the last decades the industrial needs for high performance coatings, e.g. for the tooling and machining applications, have triggered many research activities in this field. Especially, multi-layered coatings composed of layers with thicknesses of a few nm, which are called superlattice coatings if the layers grow epitaxial are very attractive. Such superlattice coatings can show at a certain bilayer period (Λ) enhanced thermal and mechanical properties [1–3]. This so called superlattice effect is most dominant for bilayer periods in the range of a few nanometres [4]. For example, the multilayer coatings TiN/AlN [5], CrN/NbN [6], CrN/$Cr_{1-x}Al_xN$ [7], TiN/NbN [2] and TiN/CrN [8] showed higher hardnesses, corrosion and wear resistance when compared to their individual monolithically grown counterparts. The increase in hardness can be explained for example by the restriction of the dislocation movement, the effect of image forces on dislocations as described by Koehler [9] and the alternating strain field in the film, which is caused by the lattice mismatch between the two materials or the modified Hall-Petch effect [10,11]. The high number of interfaces influences the properties of these coatings and is mainly responsible for the good oxidation behaviour as they act as obstacles for the elemental diffusivity in the film [12]. Due to the downsizing of the individual layer thicknesses high resolution and sensitive investigation methods like transmission electron microscopy (TEM) and nanoindentation are required to determine the crystal structure and the hardness of such superlattice coatings. Especially CrN/AlN superlattice coatings indicated improvements in thermal, mechanical, and tribological properties and oxidation resistance [1,12–16]. To achieve these desired properties, sharp interfaces and optimized layer periodicity as well as epitaxial growth is required. AlN has a stable hexagonal (ZnS-wurtzite type, w-) structure and a metastable cubic (NaCl type, c-) structure, which can be stabilized by coherency stresses if an individual layer thickness of ~3 nm is not exceeded [1,17]. If the AlN layer thickness is above ~3 nm, the thermodynamically stable wurtzite crystal structure is preferred. CrN itself crystallizes in the cubic NaCl structure, enabling the stabilization of the metastable c-AlN when grown epitaxial on CrN and preparing CrN/AlN superlattice coatings [18]. Nevertheless, a systematic study on the influence of the individual layer thicknesses of CrN and AlN on structural and mechanical properties of CrN/AlN superlattice coatings is still missing. Therefore, 17 different CrN/AlN superlattice coatings were prepared with AlN layer thicknesses of 1, 2 and 3.3 nm and varying the CrN layer thickness to obtain bilayer periods Λ between 1.9 and 12 nm. Detailed

investigations were conducted by high resolution (HR-) TEM, low angle and high angle X-ray diffraction (LAXRD and HAXRD), nanoindentation and biaxial stress measurement. Based on the results we can conclude that if the AlN layers are thinner than the CrN layers the AlN layers can not completely be stabilized by epitaxial growth in their metastable cubic structure.

Experimental

CrN/AlN superlattice coatings with modulations of the bilayer period from 1.9 to 12 nm were deposited on Si (100) substrates (7x20x0.38 mm^3) by magnetically unbalanced reactive magnetron sputtering in Ar+N_2 glow discharge. The depositions were carried out in an AJA Orion 5 lab-scaled deposition plant equipped with two 2'' Al and one 3'' Cr target (purity 99.95%). A computer-controlled system allows for sequentially switching on and off the targets to prepare coatings with different bilayer periods.

Prior to lading the samples into the deposition chamber they were ultrasonically cleaned in acetone for 5 minutes. After evacuating the chamber to a base pressure below 10^{-3} Pa the substrates were thermally cleaned at a temperature of 500 °C for 30 minutes. The depositions were carried out at 470 °C in an Ar+N_2 glow discharge with a gas flow ratio of 4/6 and a total pressure of 0.4 Pa. The two Al targets were dc-powered with 230 W and the Cr target was dc-powered with 250 W. The substrates were rf-biased with 70 V during deposition. A total thickness of ~1.5 μm for all CrN/AlN coatings independent of the superlattice period was obtained by varying the number of layers from 250 (Λ = 12.0 nm) to 1580 (Λ = 1.9 nm). For comparison also a monolithically grown CrN coating was prepared.

The structure and phase analysis as well as the bilayer periods of our CrN/AlN coatings were carried out by a Siemens X-ray diffractometer (Model D500) equipped with a Cu radiation source (K_α = 0.15406 nm) in Bragg Brentano configuration. Furthermore the bilayer periods of our CrN/AlN superlattice coatings were characterized using low-angle X-ray diffraction (LAXRD) with measuring angles from 1 to 7 deg.

Detailed investigations of the morphology of our CrN/AlN superlattice coatings were conducted in a Philips CM 12 transmission electron microscope (TEM) operating at 120 kV and a Joel high-resolution transmission electron microscope (HR-TEM) operating at 200 kV.

The mechanical properties of our CrN/AlN superlattice coatings were measured with an ultra-micro-indentation system (UMIS) equipped with a Berkovich tip. The hardness was obtained by evaluating the loading and unloading segments of the indentation curve after the Oliver and Pharr method [19]. Room temperature biaxial stresses within the films were accomplished by measuring the substrate curvature.

Results and Discussion

LAXRD and HAXRD experiments were conducted on all CrN/AlN superlattice coatings to determine the individual layer thicknesses, the bilayer period and to study their structure.

Investigation of the crystal structure and the bilayer period

Figure 1 shows the LAXRD patterns of CrN/AlN superlattice coatings with an AlN layer thickness of 1 nm and increasing CrN layer thicknesses to obtain bilayer periods Λ between 2.9 and 6.4 nm, which was calculated from the first (m = 1) to third (m = 3) order peak position θ using the modified Bragg equation [11]:

$$\Lambda = \frac{m\lambda}{2\sin(\theta)}, \qquad (1)$$

where λ is the X-ray wavelength. The first order peaks (m = 1) can clearly be identified by their sharp maximum, allowing for an accurate determination of the diffraction angle. Higher order (m = 2 and m = 3) where only used for comparison.

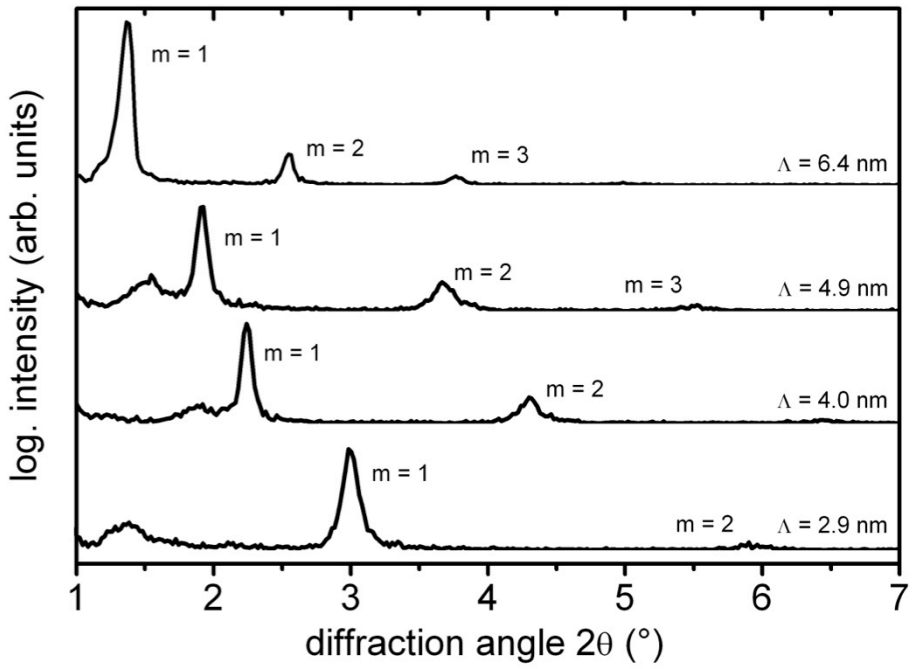

Figure 1: LAXRD patterns of CrN/AlN superlattice coatings with 1 nm thin AlN layers and bilayer periods Λ between 2.9 nm and 6.4 nm.

HAXRD (Bragg Brentano mode) patterns of our CrN/AlN superlattice coatings having an AlN layer thickness of 1 nm combined with various CrN layer thicknesses are given in Fig. 2. The patterns reveal satellite peaks on the left side of the main cubic (111) peak indicating a superlattice structure. These satellite peaks shift with increasing CrN layer thickness to higher 2θ angles and allow the calculation of the bilayer period Λ by using a modification of the Bragg equation [11]:

$$sin\theta_{\pm} = sin\theta_B \pm \frac{m\lambda}{2\Lambda}, \qquad (2)$$

where θ_B refers to the position of the main Bragg peak position and $\theta_{\pm}$ to the position of the satellite peak. The bilayer periods determined by HAXRD are in an excellent agreement to those obtained by LAXRD. Furthermore, the HAXRD patterns also give information on the crystal structure of our CrN/AlN superlattice coatings.

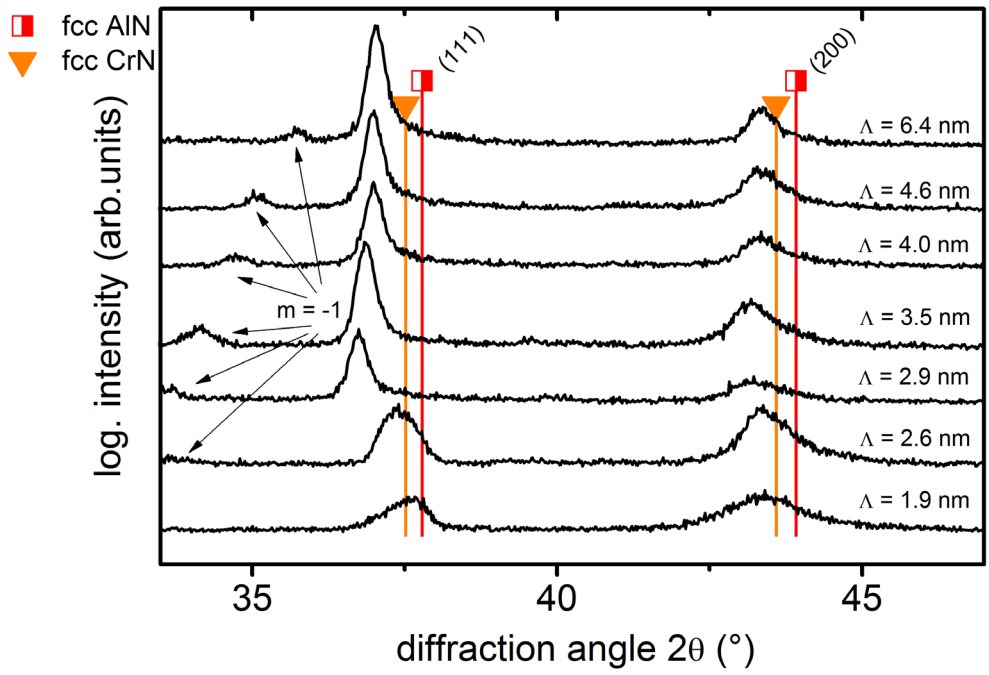

Figure 2: HAXRD patterns of CrN/AlN superlattice coatings composed of 1 nm thin AlN layers.

The CrN/AlN superlattice coatings with 1 nm thin AlN layers (see Fig. 2) reveal only a cubic crystal structure, indicated by the XRD peaks near the 2θ position for c-CrN at 2θ = 37.516° (111) and 2θ = 43.594° (200) [20] and c-AlN at 2θ = 37.785° (111) and 2θ = 43.917° (200) [21]. As the 2θ positions for c-CrN and c-AlN are very close, their XRD response overlaps which can especially be seen by the asymmetric shape of the (200) XRD peak at 2θ ~43°. The shift of the cubic XRD peaks towards lower diffraction angles as compared to the standard position for c- CrN and c-AlN can clearly be seen and suggests compressive stresses. Consequently, the XRD results indicate that the compressive stresses first increase within increasing CrN layer thickness to reach a maximum for the coating with Λ = 2.9 nm and then decrease again.

Figure 3 shows the HAXRD patterns of the CrN/AlN superlattice coatings composed of 2 nm thin AlN layers and varying CrN layer thicknesses. Based on Eq. (2) their bilayer period ranges from 3.5 to 12 nm.

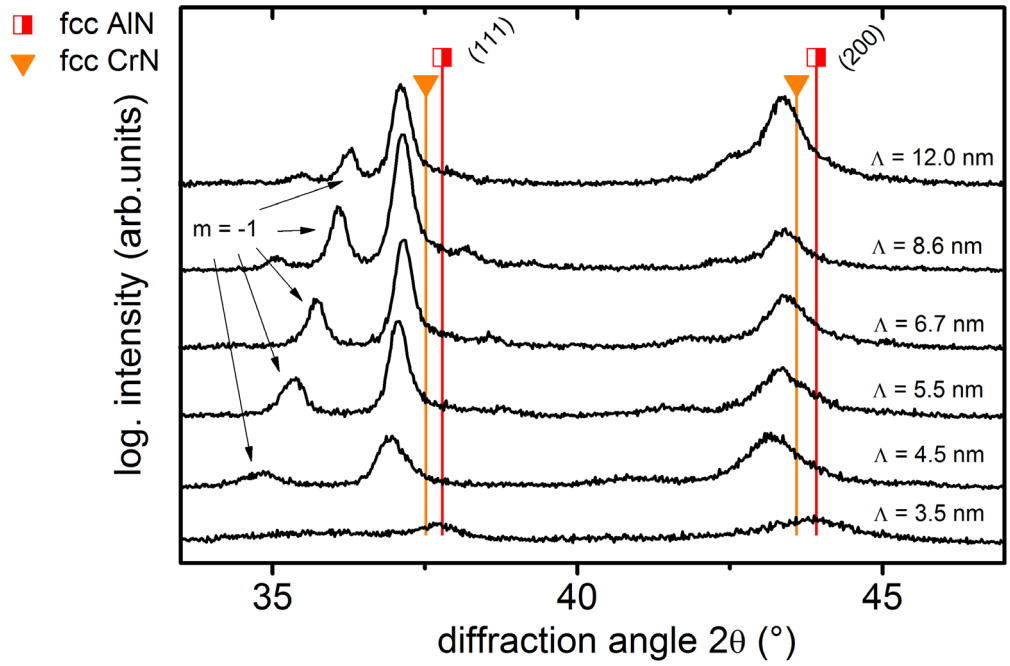

Figure 3: HAXRD patterns of CrN/AlN superlattice coatings composed of 2 nm thin AlN layers.

The superlattice coating with the thinnest CrN layer (Λ = 3.5 nm) exhibits no well-defined XRD peaks suggesting that here the CrN layer is too thin (~1.5 nm) to allow for a complete strain-induced stabilization (by epitaxial growth) of the AlN phase in its metastable cubic structure. Increasing the CrN layer thickness (and hence the bilayer period of these coatings with 2 nm thin AlN layers) leads to a well-defined crystalline cubic structure. Furthermore, first order satellite peaks are clearly detectable. For the coatings with Λ = 8.5 and 12.0 nm even second order satellite peaks can be identified. The superlattice coating with Λ = 4.5 nm exhibits the largest deviation of the cubic XRD peaks from the standard position for c-CrN and c-AlN, which also suggest the highest compressive stresses.

The HAXRD patterns of the CrN/AlN superlattice coatings composed of 3.3 nm thin AlN layers and various CrN layer thicknesses are given in Fig. 4. Based on Eq. 2 and LAXRD measurements the bilayer period of these coatings ranges from 4.2 to 8.3 nm.

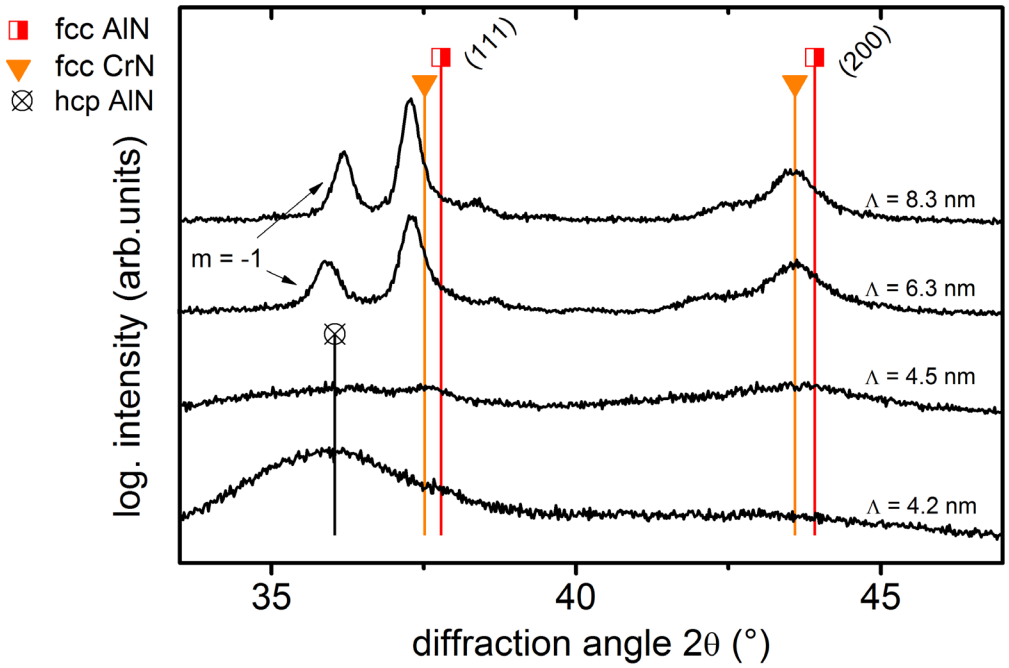

Figure 4: HAXRD patterns of CrN/AlN superlattice coatings composed of 3.3 nm thin AlN layers.

The coatings with 0.9 and 1.2 nm thin CrN layers (Λ = 4.2 and 4.5 nm) have no well-defined crystalline structure. For CrN layer thicknesses above 3 nm (Λ = 6.3 nm) the 3.3 nm thin AlN layers can be stabilized in their metastable cubic structure. These superlattice coatings exhibit a single-phase cubic structure with well-defined satellite peaks. The results obtained for the individual coatings composed of 1, 2, or 3.3 nm thin AlN layers indicate that the c-CrN layers need to be at least as thick as the AlN layers for an effective strain-induced stabilization in their metastable cubic structure.

Microstructure of CrN/AlN superlattice coatings

The cross-sectional (HR-) TEM images of our CrN/AlN superlattice coatings with 1 nm AlN and 2 nm CrN, see Fig. 6, confirm the calculated layer thicknesses for the AlN and CrN layers. The coating exhibits a dense morphology with 20–40 nm wide columns, see Fig. 6a, and sharp and well defined interfaces between the AlN and CrN layers, see Fig. 6b. The darker contrast indicates the CrN layers as the Cr atoms exhibit a higher scattering factor as compared to Al.

Especially, the HRTEM image in Fig. 6c nicely presents the continuing lattice fringes passing through the AlN and CrN layers and confirms the single-phase cubic structure as suggested by HAXRD pattern presented in Fig. 2.

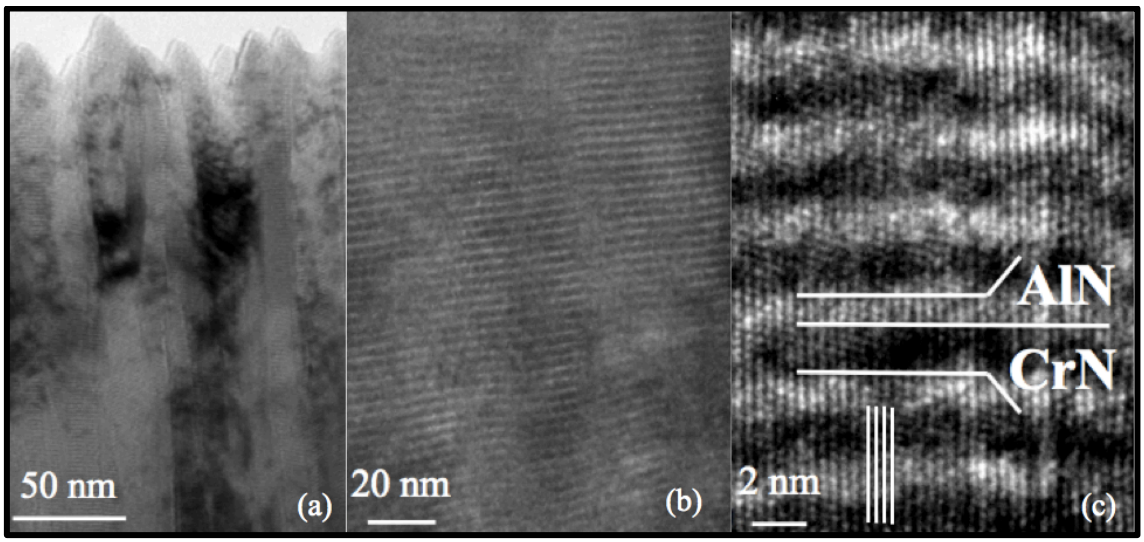

Figure 6: (HR -) TEM cross-section of the superlattice coating with 1 nm thin AlN and 1.9 nm thin CrN layers. (a) Overview image showing the columnar growth, (b) layer arrangement with darker contrast for the CrN layers, and (c) epitaxial growth of AlN and CrN layers without misfit dislocations in the presented area.

Mechanical properties – Hardness and stresses

Figures 8 and 9 show the profile of hardness and stresses of all CrN/AlN coatings investigated as a function of their bilayer period Λ. The hardness and stresses of monolithically grown CrN were evaluated for comparison and were found to be ~22 GPa and ~ -969 MPa, respectively. The hardness profile of the CrN/AlN superlattice coatings with 1 nm AlN and 2 nm thin AlN layers exhibit a pronounced peak at ~31 GPa for Λ = 2.9 nm and Λ = 5.5 nm, respectively. The superlattice coatings composed of 3.3 nm thin AlN layers have a lower hardness maximum of ~28.5 GPa at Λ = 6.3 nm. The peak hardness is obtained nearly at the minimum bilayer periods (or actually CrN layer thicknesses) necessary to stabilize the 1, 2, or 3.3 nm thin AlN layers in their metastable cubic structure. The superlattice coatings with thinner CrN layers exhibit an X-ray amorphous structure or contain even wurtzite-like phases, cf. Figs. 2-4. For thicker CrN layers the density of AlN/CrN interfaces decreases, and also dislocation movement within the CrN layers becomes easier. Consequently, the hardness decreases again. This was also shown by modelling of TiN/NbN layers [22]. Furthermore, the

comparison of the individual CrN/AlN layer systems nicely shows that the hardness peak becomes sharper with decreasing AlN layer thickness.

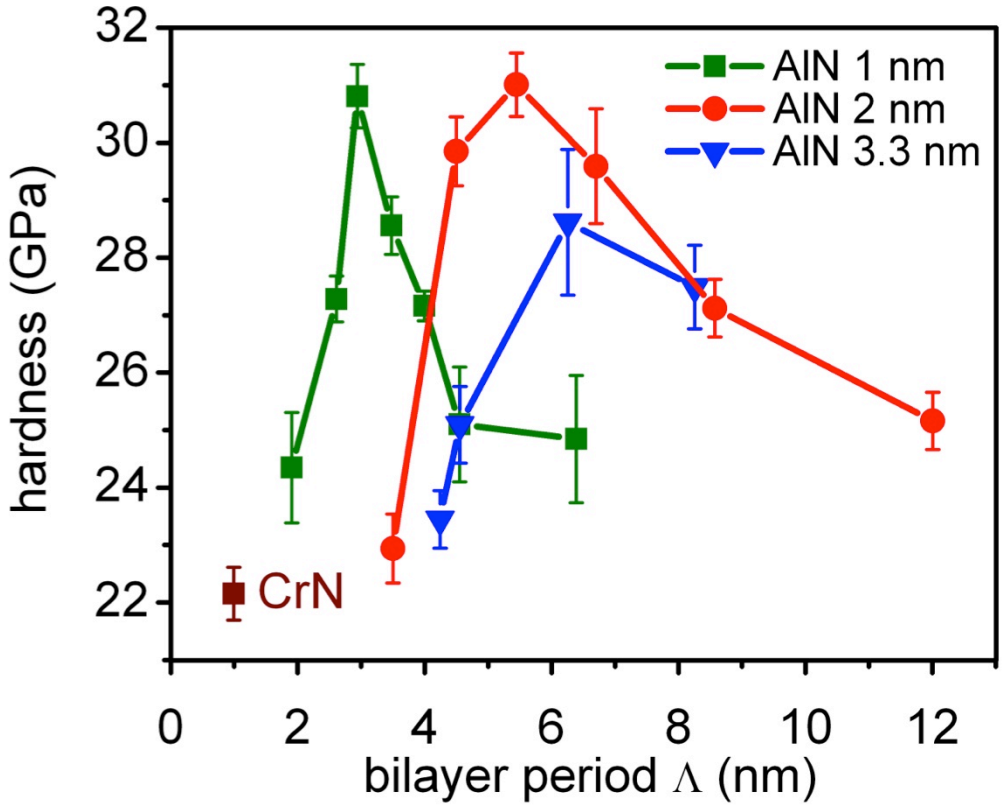

Figure 8: Hardness as a function of the bilayer period Λ (or CrN layer thickness) for our CrN/AlN coatings composed of 1, 2, and 3.3 nm thin AlN layers.

The so-called superlattice effect leads to a hardness increase up to 140% when compared to monolithically grown CrN coatings. The superlattice effect on hardness is based on various aspects, such as Koehler's effect, the effect of image forces on dislocation, hindering of dislocation propagation due to epitaxial-strains between the individual layers (in our case CrN and AlN), or the Hall-Petch effect [9–11,23]. With increasing shear moduli difference between the alternating layers the dislocation propagation becomes more difficult, giving rise to the observed hardness increase. Dislocations are more easily generated in the layers having lower shear moduli, in our case c-CrN. Ab initio calculations suggest shear moduli values of ~140 GPa for c-CrN [23], ~220 GPa for c-AlN [24], and ~116 GPa for w-AlN [25]. To propagate dislocations from the lower-shear-moduli-layer to the higher-shear- moduli-layer (i.e., from c-CrN to c-AlN) additional strains are necessary. In addition, coherency-strains

between the lattice-mismatched layers also provide obstacles for dislocation movement, as described by Yashar et al [11].

The biaxial-stresses of our CrN/AlN coatings composed of 1, 2, or 3.3 nm thin AlN layers exhibit a similar dependence on their bilayer period Λ, Fig. 9, as the hardnesses, Fig. 8. The peak-stresses (compression) are close or at the bilayer period (i.e. CrN layer thicknesses) where also the peak-hardnesses are obtained. Furthermore, with decreasing AlN layer thicknesses the peak- formation becomes sharper and the stress-profiles are shifted to lower values. Consequently, with increasing CrN phase fraction the compressive stresses decreases, except for the coatings exhibiting an X-ray amorphous structure or containing wurtzite-like phases.

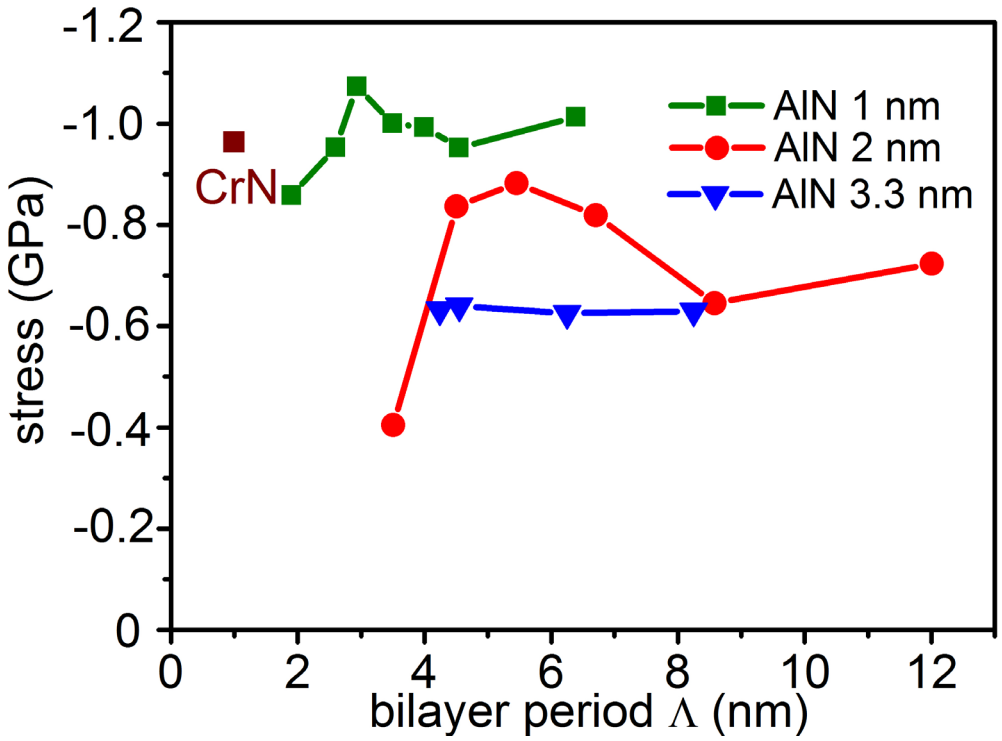

Figure 9: Stress Biaxial stresses as a function of the bilayer period Λ (or CrN layer thickness)for our CrN/AlN coatings composed of 1, 2, and 3.3 nm thin AlN layers.

Conclusions

To study in detail the influence of the individual layer thicknesses of CrN and AlN on the structural and mechanical properties of CrN/AlN coatings, different variations were prepared by DC reactive magnetron sputtering. For AlN layer thicknesses of 1, 2 and 3.3 nm the corresponding CrN layer thicknesses were varied between 0.9 and 10 nm. Thereby, CrN/AlN coatings with bilayer periods Λ between 1.9 and 12 nm are formed. Based on the results obtained we can conclude that the minimum CrN layer thickness necessary to stabilize the AlN layers in their metastable cubic structure corresponds to the AlN layer thickness. Hence, for the systems with 1, 2, and 3.3 nm thin AlN layers the minimum CrN layer thickness is 1, 2 and ~3 nm, respectively. For thinner CrN layers the coatings exhibit an X-ray amorphous structure or even wurtzite-like phase contents suggesting that these thin CrN layers are too weak to stabilize the AlN layers in their metastable cubic structure. A pronounced superlattice response (e.g., satellite peaks during HAXRD investigations) could only be detected for the CrN/AlN coatings composed of 1, 2, and 3,3 nm thin AlN layers if their bilayer periods are above 2.9, 4.5, and 6.3 nm, respectively. Cross-sectional HRTEM investigations of the coating composed of 1 nm thin AlN and 1.9 nm thin CrN layers (Λ = 2.9 nm) confirm the superlattice structure by the almost perfect hetero-epitaxial relationship between c-CrN and c-AlN.

With increasing AlN layer thickness, also the hardness-peak as a function of the bilayer period becomes broader. Whereas the CrN/AlN coatings composed of 1 nm thin AlN layers exhibit a distinct hardness peak with 31 GPa at Λ = 2.9 nm (hardnesses below 27 GPa for $\Lambda \leq$ 2.6 or 28 GPa for $\Lambda \geq$ 3.5 nm) the hardness maximum for the other coatings covers a broader bilayer period. The CrN/AlN coatings with 2 nm thin AlN layers have their hardness peak with 31 GPa at Λ = 5.5 nm, but have hardnesses of ~29.5 GPa also for Λ = 4.5 and 6.7 nm. If the AlN layer thickness is ~3.3 nm the maximum hardness obtained is only ~28 GPa for Λ = 6.3 nm. Consequently, the arrangement of 1 nm thin AlN layers with 1.9 nm thin CrN layers or 2 nm thin AlN layers with 3.5 nm thin CrN layers into a superlattice CrN/AlN structure leads to a pronounced hardness increase up to ~140 % of the individual layers. The structural behaviour of our CrN/AlN superlattice coatings showed, that just above a certain layer thickness of c-CrN epitaxial growth with c-AlN is achievable and the mechanical properties, in particular the hardness was improved compared to monolithically grown CrN.

Bibliography

[1] J.-K. Park, Y.-J. Baik, Surface and Coatings Technology 200 (2005) 1519–1523.

[2] L. Hultman, C. Engström, M. Odén, Surface and Coatings Technology 133-134 (2000) 227–233.

[3] X.T. Zeng, Surface and Coatings Technology 113 (1999) 75–79.

[4] W.D. Sproul, Surface and Coatings Technology 86-87 (1996) 170–176.

[5] M. Setoyama, A. Nakayama, M. Tanaka, N. Kitagawa, T. Nomura, Surface and Coatings Technology 87 (1996) 225–230.

[6] D.C. Cameron, R. Aimo, Z.H. Wang, K.A. Pischow, Surface and Coatings Technology (2001) 567–572.

[7] Y.J. Kim, T.J. Byun, J.G. Han, Superlattices and Microstructures 45 (2009) 73–79.

[8] Q. Yang, C. He, L.R. Zhao, J.-P. Immarigeon, Scripta Materialia 46 (2002) 293–297.

[9] K. J.S., Physical Review 2 (1970) 547–551.

[10] S. Veprek, R.F. Zhang, M.G.J. Veprek-Heijman, S.H. Sheng, a. S. Argon, Surface and Coatings Technology 204 (2010) 1898–1906.

[11] P.C. Yashar, W.D. Sproul, Materials Science 55 (1999) 179–190.

[12] J. Lin, J.J. Moore, J. Wang, W.D. Sproul, Thin Solid Films 519 (2011) 2402–2408.

[13] G.S. Kim, S.Y. Lee, J.H. Hahn, Surface and Coatings Technology 171 (2002) 91–95.

[14] J. Lin, J.J. Moore, B. Mishra, M. Pinkas, W.D. Sproul, Surface and Coatings Technology 204 (2009) 936–940.

[15] J. Lin, J.J. Moore, B. Mishra, M. Pinkas, X. Zhang, W.D. Sproul, Thin Solid Films 517 (2009) 5798–5804.

[16] S.-K. Tien, J.-G. Duh, Thin Solid Films 494 (2006) 173–178.

[17] F.H. Mei, N. Shao, J.W. Dai, G.Y. Li, Materials Letters 58 (2004) 3477–3480.

[18] M. Setoyama, A. Nakayama, M. Tanaka, N. Kitagawa, T. Nomura, Surface and Coatings Technology 86-87 (1996) 225–230.

[19] W.C. Oliver, G.M. Pharr, (1992).

[20] Powder Diffraction File 03-065-2899, International Center for Diffraction Data, PDF-2/Release 2007, n.d.

[21] Powder Diffraction File 00-025-1495, International Center for Diffraction Data, PDF-2/Release 2007, n.d.

[22] A. Madan, P. Yashar, M. Shinn, S.A. Barnett, Thin Solid Films 302 (1997) 147–154.

[23] L. Zhou, D. Holec, P.H. Mayrhofer, (2012) 24.

[24] D. Holec, M. Friák, J. Neugebauer, P. Mayrhofer, Physical Review B 85 (2012).

[25] S. Łepkowski, J. Majewski, G. Jurczak, Physical Review B 72 (2005).